



저작자표시-비영리-변경금지 2.0 대한민국

이용자는 아래의 조건을 따르는 경우에 한하여 자유롭게

- 이 저작물을 복제, 배포, 전송, 전시, 공연 및 방송할 수 있습니다.

다음과 같은 조건을 따라야 합니다:



저작자표시. 귀하는 원저작자를 표시하여야 합니다.



비영리. 귀하는 이 저작물을 영리 목적으로 이용할 수 없습니다.



변경금지. 귀하는 이 저작물을 개작, 변형 또는 가공할 수 없습니다.

- 귀하는, 이 저작물의 재이용이나 배포의 경우, 이 저작물에 적용된 이용허락조건을 명확하게 나타내어야 합니다.
- 저작권자로부터 별도의 허가를 받으면 이러한 조건들은 적용되지 않습니다.

저작권법에 따른 이용자의 권리는 위의 내용에 의하여 영향을 받지 않습니다.

이것은 [이용허락규약\(Legal Code\)](#)을 이해하기 쉽게 요약한 것입니다.

[Disclaimer](#)

Thesis for the Degree of Master of Science

Realization of practical sheet-type biosensor
based on multi wall carbon nanotubes and
micro-pore filter paper for early detection of
prostate cancer



By

Sung Kyung Ji

Department of Chemistry

The graduate school

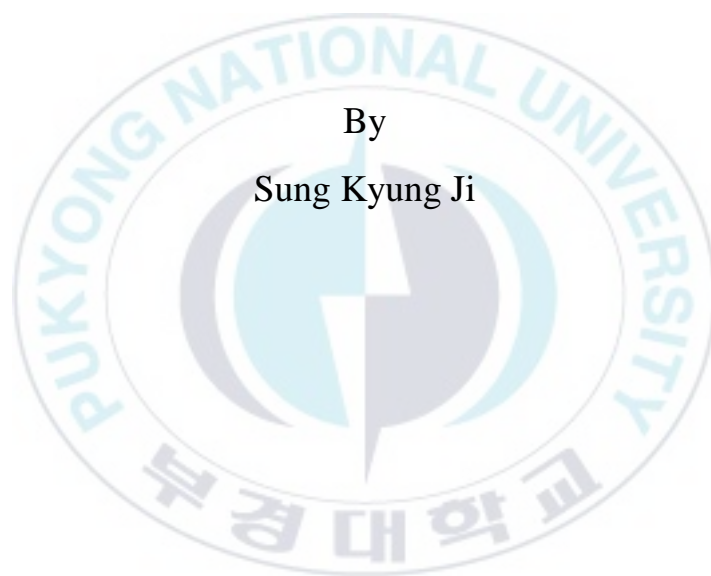
Pukyong National University

August 2015



Realization of practical sheet-type biosensor based on multi wall carbon nanotubes and micro-pore filter paper for early detection of prostate cancer

Advisor: Prof. Don Kim



By
Sung Kyung Ji

A thesis submitted in partial fulfillment of the requirements

For the degree of Master of Science

In Department of Chemistry, The Graduate School,

Pukyong National University

August 2015

Realization of practical sheet-type biosensor based on multi wall carbon nanotubes and micro-pore filter paper for early detection of prostate cancer

A dissertation

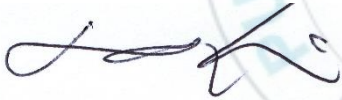
By

Sung Kyung Ji

Approved by:



(Chairman) Degree of Ph.D., Byoung-Yong Chang



(Member) Degree of Ph.D., Don Kim



(Member) Degree of Ph.D., Minseok Kwak

August 21, 2015

Table of Contents

List of Scheme	ii
List of Figures	iii
List of Tables	vi
Abstract	vii
1. Introduction	1
2. Experimental section	11
2.1 Materials	11
2.2 Fabrication of biosensor based on carboxylated MWCNTs	12
2.3 Fabrication of biosensor based on Au-MWCNTs	15
2.4 Commercial ELISA kit performance test	19
3. Results and discussion	20
3.1 Fabrication of biosensor based on carboxylated MWCNTs	20
3.2 Fabrication of biosensor based on Au-MWCNTs	36
3.3 Commercial ELISA kit performance test	59
4. Conclusion	61
5. References	63

List of Schemes

Scheme 1.	Preparation of the activated MWCNTs with PSA antibody. Incubated at 37 °C for 1.5 h.	14
Scheme 2.	Preparation of sensor element and PSA detection procedure.	14
Scheme 3.	Preparation of gold nanoparticles attached MWCNTs for fabrication of PSA detectable sensor element.	17
Scheme 4.	PSA detection process and biosensor assembly.	18
Scheme 5.	Strategy for cutting to exact size ($5 \times 2 \text{ mm}^2$) of sensing paper and preservation of sensing materials in wet.	26
Scheme 6.	PSA detection process and assembly of biosensor.	27

List of Figures

Figure 1.	Direct ELISA method.	7
Figure 2.	Indirect ELISA method.	7
Figure 3.	Sandwich ELISA method.	8
Figure 4.	Competitive ELISA method.	9
Figure 5.	Different forms of SWCNTs. (A) The chiral vector C also determines the tube diameter. (B) Models of three atomically perfect SWCNT structures.	10
Figure 6.	FT-IR spectra of MWCNTs, carboxylated MWCNTs and Ab-MWCNTs. ...	21
Figure 7.	(a) is SEM image, and (b) is AFM image of carboxylated MWCNTs. (c) is SEM image, and (d) is AFM image of Ab-MWCNTs. (e) is SEM image, and (f) is AFM image of PSA-Ab-MWCNTs. Scanned area of AFM images is $1.3 \times 1.3 \mu\text{m}^2$	23
Figure 8.	Height profile measured by alpha-step. Thickness of Ab-MWCNTs layer in sensing paper was measured after removing the filter paper.	28
Figure 9.	(a) and (b) show the ways to cut the sensing element. (c) Relative electrical resistance value for respective sample.	29
Figure 10.	I-V curves for MWCNTs, activated MWCNTs with carboxyl group, Ab-MWCNTs and PSA-Ab-MWCNTs in the current range of $\pm 1.40 \text{ mA}$ (a) and $\pm 1.00 \mu\text{A}$ (b).	31
Figure 11.	The electrical resistance of MWCNTs, carboxylated MWCNTs, Ab-MWCNTs and PSA-Ab-MWCNTs (PSA: 1000 ng/mL).	32

Figure 12.	The plot of relative resistance vs. PSA concentration. For (a) wide range of PSA concentration (0-1000 ng/mL) and (b) low level of PAS (0-10 ng/mL).	34
Figure 13.	Electrical signal of background to determine the detection limit.	35
Figure 14.	TEM image of the Au NPs and abundance ratio according to particles size. (a), (c) unaged Au NPs (size: 3.6 ± 0.7 nm) and (b), (d) aged Au NPs (size: 4.6 ± 0.9 nm) for 12 days.	37
Figure 15.	UV-Vis spectra of (a) Au NPs for unaged Au NPs and (b) 12 days aged Au NPs. The absorbance peak of unaged Au NPs became red shift by aging effect of Au NPs.	38
Figure 16.	FT-IR spectra of MWCNTs, carboxylated MWCNTs and thiolated MWCNTs.	41
Figure 17.	TEM images of the (a) Au NPs attached carboxylated MWCNTs and (b) Au NPs attached thiolated MWCNTs.	42
Figure 18.	TEM images of the (a) Au NPs attached carboxylated MWCNTs and (b) Au NPs attached thiolated MWCNTs.	43
Figure 19.	FT-IR spectra of carboxylated MWCNTs with different reflux time.	45
Figure 20.	FT-IR spectra of carboxylated MWCNTs according to reflux in different concentration of nitric acid.	46
Figure 21.	UV-Vis spectra of prepared Au NPs at 0 °C and room temperature.	47
Figure 22.	Photograph of prepared Au NPs solution.	48
Figure 23.	(a) is UV-Vis spectra of sample 1, 2 and 3. (b) is UV-Vis spectrum of sample 2 magnified from Figure 23(a). Total volume of prepared Au NPs solution was 5 mL.	49
Figure 24.	UV-Vis spectra of prepared Au NPs solution in bulk (200 mL).	51

Figure 25.	(a) is TEM image obtained from high concentration Au NPs solution in bulk. (b) is size distribution of Au NPs. (Au NPs size : 5.2 ± 1.2 nm).	52
Figure 26.	(a) and (b) are TEM images of Au NPs attached MWCNTs. (c) shows crystal lattices of Au NPs and MWCNT wall. (d) is SAED image of Au NPs.	53
Figure 27.	Compared specific gravity between carboxylated MWCNTs and Au-MWCNTs.	55
Figure 28.	Height profile measured by alpha-step. Thickness of Ab-Au-MWCNTs layer measured after removing the filter paper.	56
Figure 29.	Electrical signal of background to determine the detection limit.	57
Figure 30.	The plot of relative resistance vs. PSA concentration. PSA concentration is 0, 10, 100, 250, 500 and 1000 ng/mL.	58
Figure 31.	(a) Optical density of ELISA method at 450 nm vs. PSA concentration. (b) Linear range of signal along with PSA concentration at ELISA method.	60

List of Tables

- Table 1.** The relative resistances of MWCNTs, carboxylated MWCNTs, Ab-MWCNTs, and PSA-Ab-MWCNTs, those are estimated from the Figure 10. **32**
- Table 2.** The amount of reagents to prepare the Au NPs solution. The total volume of the solution is 5 mL. **48**



Realization of practical sheet-type biosensor based on multi wall carbon nanotubes and micro-pore filter paper for early detection of prostate cancer

Sung Kyung Ji

Department of Chemistry, The Graduate School,
Pukyong National University

Abstract

The aim of this study is realization of an inexpensive, simple and sensitive biosensor to detect early stage of prostate cancer using multi wall carbon nanotubes (MWCNTs, diameter 20 nm, length 5 μm) and micro-pore filter paper (pore size 0.45 μm). For the detection of prostate specific antigen (PSA), which is a biomarker of prostate cancer, the carboxylated MWCNTs were activated with PSA antibody (monoclonal antibody of the prostate specific antigen) by using N-(3-dimethylaminopropyl)-N'-ethylcarbodiimide hydrochloride (EDC) and N-hydroxysulfosuccinimide sodium salt (NHSS). The activated MWCNTs were deposited on micro-pore filter paper by using syringe filtering. The biosensor can detect from 0 to 500 ng/mL of PSA level within 90 min with high sensitivity: the signal (electrical resistance) increased up to 150% of the base signal along with the increased concentration of PSA from 0 to 500 ng/mL and the detection limit was 1.18 ng/mL with a bench top digital multimeter (6 1/2 digits). The detection limit of biosensor is enough to diagnose prostate cancer. Because they are suspected to patients of prostate cancer when PSA level in serum is more than 4 ng/mL. Our sensing system is much simple,

fast and cheap, but the detection ability of the sensor is comparable to that of commercially available methods. In case of enzyme-linked immunosorbent assay (ELISA) that is conventional method for quantitative analysis of proteins, detection limit was 51 pg/mL.

In order to improve performance of the biosensor, MWCNTs were refluxed in concentrated 14 M nitric acid instead of 3 M nitric acid. Then thiolation of the carboxylated MWCNTs was conducted by 2-aminoethanethiol hydrochloride and gold nanoparticles (Au NPs, diameter ~5 nm) were attached by self-assembly (SA) on the surface of thiolated MWCNTs. For the reaction of Au NPs and PSA antibody, citrate that is capping agent of Au NPs was replaced with thioglycolic acid by ligand exchange process. Thiol group in thioglycolic acid was bonded to Au NPs and carboxyl group in thioglycolic acid was used to combine PSA antibody and Au-MWCNTs. Fabrication of biosensor based on Au-MWCNTs and PSA detection were carried out in the same manner as fabrication of carboxylated MWCNTs based biosensor. The Au-MWCNTs based biosensor need additional research and development to improve the performance.

1. INTRODUCTION

Prostate cancer is one of the popular cancer and second leading cause of cancer deaths among men in the United states.¹ According to a recent report,² the incidence rate of prostate cancer in Korea is 27 per 100,000 people. That is lower than in the United States, but the incidence rate is steadily increased recently along with the change of their daily life. Therefore, prostate cancer might be a major cancer in Korea and other underdevelopment countries not far future. However, if the early detection of prostate cancer, the survival rate for 5 years is about 98.9%.^{3,4} Therefore the detection of the early stage of cancer is extremely important in order to ensure a successful treatment and high survival rate.

One way for the early detection of the cancer is detection and quantification of ultralow level biomarker by using a specialized analysis. The term "biomarker" is a portmanteau word of "biological marker" and refers to a broad category of medical signs that is indications of medical state observed from medical examination of the patients.⁵ In other words, the biomarker is an indicator that shows any changes in human body by using proteins, sugars, lipids, DNA, RNA and metabolites etc. Especially, biomarkers of cancer are proteins overexpressed in blood and serum or at the epithelial cells of organs when cancer is developed. In case of prostate cancer, prostate specific antigen (PSA) corresponds to the biomarker.⁶

PSA (also known as kallikrein III, semenogelase, γ -seminoprotein, seminolisin and P-30 antigen) that is a 34 kD glycoprotein produced almost exclusively by the prostate gland was first identified by researchers attempting to find a substance in seminal fluid that would aid in the investigation of rape cases in 1971.⁷ PSA was first successful in

quantitative analysis in the blood by Papsidero and colleagues in 1980. They are also reported clinical use as a marker of prostate cancer.⁸ Currently, PSA is the most commonly studied biomarker in prostate cancer and useful biomarker for detection of prostate cancer because among all kallikreins, human kallikrein gene 3 and human glandular kallikrein expression is highly restricted to the prostate in males. PSA of small quantities are detected in the serum of normal men. However, amount of PSA is increased in the presence of prostate cancer and other prostate disorders. Therefore the high level of PSA in a patient serum (> 4.0 ng/mL) indicates the incidence of the prostate cancer.⁹

One of the most common quantitative analysis methods of biological substance is the enzyme-linked immunosorbent assay (ELISA). ELISA is a test which uses antibody and color change to identify an analyte. In 1971, Peter Perlmann and Eva Engvall first demonstrated ELISA for quantitative analysis of IgG in rabbit serum and reported their achievements.¹⁰ Basic principle of ELISA is as follows. Antigens from the sample are attached on the surface of plate, and the specific antibodies are applied over the surface. Consequently, the antibodies are bound to the antigens. This antibodies are bound to enzymes and substance containing the substrate of enzyme is added. The subsequent reaction produces the detectable signal which is usually a color change in the substrate. The type of ELISA is divided into direct ELISA, indirect ELISA, sandwich ELISA and competitive ELISA (shown in Figure 1~4, respectively). Among the four types, sandwich ELISA currently is the most used method and has been utilized as a method for the PSA detection.^{11,12} However, this conventional method used in hospital is time consuming (approximately 1 day), uneconomical (approximately 55 \$ per test) procedure, which should be performed in a well-equipped laboratory.¹³ Therefore, the realization of smart biological detection system, which can detect the PSA very fast by

a simple and inexpensive method, will be a great advanced step to increase the survival rate of the prostate cancer patients.

The term "biosensor" is short for "biological sensor". The biosensor for detection of biological molecules consist of transducers and electronic systems. The transducers are combination of bioreceptors and electrical interface. The bioreceptors include antibodies, nucleic acids, cells and enzymes etc. The electrical interface usually is a device form such as field effect transistor, nanowire array, nanoparticles and electrodes etc. The electronic systems carry out signal amplification and transformation of signal. The biosensor attracts interest and is being briskly researched because of outstanding advantages of the biosensor such as fast detection time, high sensitivity, small size of the device and reasonable cost.

Actually, there have been many reports for the miniaturization and the improved performance of the biosensor.¹⁴⁻¹⁸ One of the most promising sensors is carbon nanotubes (CNTs) based biosensor. The structure of CNTs is different from traditional carbon fibers and graphene. The CNTs consist of sp^2 carbon units and seams like hexagonal honeycomb lattices. Also, the CNTs have tubular structure and typically diameter of several nanometers and length of several microns. CNTs have two main types that is single wall carbon nanotubes (SWCNTs) and multi wall carbon nanotubes (MWCNTs). SWCNTs comprise a single graphene sheet seamlessly wrapped into a cylindrical tubes.¹⁹ MWCNTs consist of an array of such nanotubes which are concentrically nested like rings of a tree trunk. In spite of structural similarity to the single sheet of graphene, that is a semiconductor with zero band gap, SWNTs may be either semiconducting or metallic, depending on graphene sheet rolled direction to form the nanotube cylinder. The structure of SWCNTs is decided by a pair of indices (n, m).²⁰ The integers n and m denote the number of unit vectors along two directions in

the honeycomb crystal lattice of graphene. If $n=m$, the nanotubes are named armchair nanotubes, and if $m=0$, the nanotubes are named zigzag nanotubes, and other state are named chiral nanotubes (shown in Figure 5). The structure of SWCNTs is an important because most of properties are significantly changed by the (n, m) values. In particular, band gap of SWCNTs can vary from zero to approximately 2 eV. Consequently, their electrical conductivity can show metallic or semiconducting properties. Contrastively, all MWCNTs have metallic properties.²¹

Since their discovery in 1991,²² CNTs have attracted increasing interest for potential applications in electron field emitters, field-effect transistors, actuators, and sensors etc. Besides, CNTs are used in many ways such as composite materials, coatings, films, microelectronics, energy storage, environment and biotechnology²³ because of their special geometry and unique chemical, mechanical, electronic, and thermal properties.^{21,24,25} The unique properties in particular, such as high chemical stability, electrical conductivity, mechanical strength, aspect ratio and larger surface, of CNTs make them extremely suitable for developing biosensors.²⁶⁻²⁸ Actually, for the early detection of prostate cancer, many research teams have demonstrated the biological sensing based on the CNTs; the electrochemical method based on ionic liquid-CNTs modified electrode,²⁹ electrochemiluminescence method based on quantum dots attached CNTs,³⁰ and carbon nanotube field-effect transistor (CNTFET).³¹ The detection limit of these biosensors reach from 1.0 ng/mL to 0.61 pg/mL levels. Although those biosensors represent high sensitivity and fast detection time, they have disadvantages such as high cost, complexity and laboratory-oriented experiment.

To avoid these weak point of CNTs based biosensor, there was a remarkable claim by Jack Thomas Andraka. He was awarded the 2012 Gordon E. Moore Award for his

work in developing a new, rapid and inexpensive biosensor based on the CNTs and filter paper for early detection of pancreatic cancer. According to Andraka, it is over 90 percent accurate in detecting the presence of mesothelin and 168 times faster, 26,000 times less expensive (costing around three cents), over 400 times more sensitive than the current diagnostic tests and only takes five minutes to run.³² He says the test is also effective for detecting ovarian and lung cancer, due to the same mesothelin biomarker they have in common. However, none of Andraka's work has so far been published in a peer-reviewed journal. Many of Andraka's claims do not stand up to rigorous peer-reviewed research. For instance, an article published by Sharon et al.³³ refutes many of Andraka's claims about specificity of using mesothelin as a biomarker for pancreatic cancer. Specifically, the group showed that mesothelin serum levels in healthy donors 0.58 (0.15-0.72) nmol/L were not statistically different from serum levels in pancreatic cancer patients 0.66 (0.52-0.94) nmol/L. In addition to this issue of false positives, George M. Church, has raised concern about all of main claims of the Andraka - cost, speed, and sensitivity.³⁴

It is well known that the CNTs are p-type narrow gap semiconductor in the ambient air owing to the charge transfer from CNTs to oxygen, water and other adsorbed chemicals.³⁵ The same charge transfer occurs also at the interface of metal and CNTs. Therefore, if biomolecules attached on the CNTs can withdraw electrons from CNTs, the increased holes in CNTs will enhance the electrical conductivity. On the other hand, the electrical transport properties of CNTs greatly related to the contact potential between conducting CNTs if the concentration of charge carriers is constant. Therefore, if the CNTs are coated by insulation layer (i.e. biomolecules) without charge transfer between CNTs and biomolecules, the electrical conductivity of the total system will be decreased. These two simple basic quantitative effects to electrical conductivity of the

system are the basic theory for the bio-detection. There are already some reports showing that the resistivity of the biomolecules-CNTs hybrid structure can be modulated by the amount of the attached biomolecules.^{36,37}

In this work, we report the fabrication of the sensitive, inexpensive and simple biosensor to detect early stage of prostate cancer. The biosensor was prepared by PSA antibody attached multi wall carbon nanotubes (MWCNTs) deposited micro-pore filter paper. The detection limit of the biosensor was 1.18 ng/mL. This detection limit is enough to diagnosis early state of prostate cancer.

The metal nanoparticles have been used to improve the performance of sensor materials.³⁸ The quantum dots and gold nanoparticles (Au NPs) were generally utilized as the label of the secondary antibody for delivery of optical signals and intensification of sensitivity.^{16,39-42} Also Au NPs used as a bridge between electrode and antibody.^{43,44} We thought the performance improvement of biosensor by the attached Au NPs, but there was little improvement in sensitivity. This method will be a very useful diagnosis tool for various fatal diseases in underdevelopment countries or hinterland, where modernized medical system is not provided, not far future.

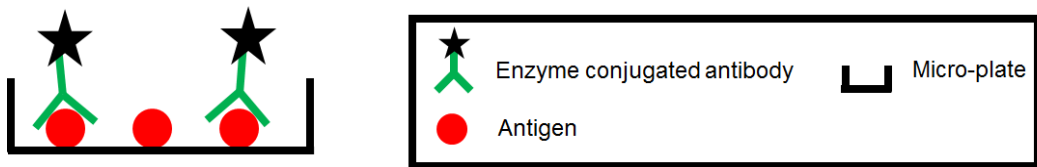


Figure 1. Direct ELISA method.

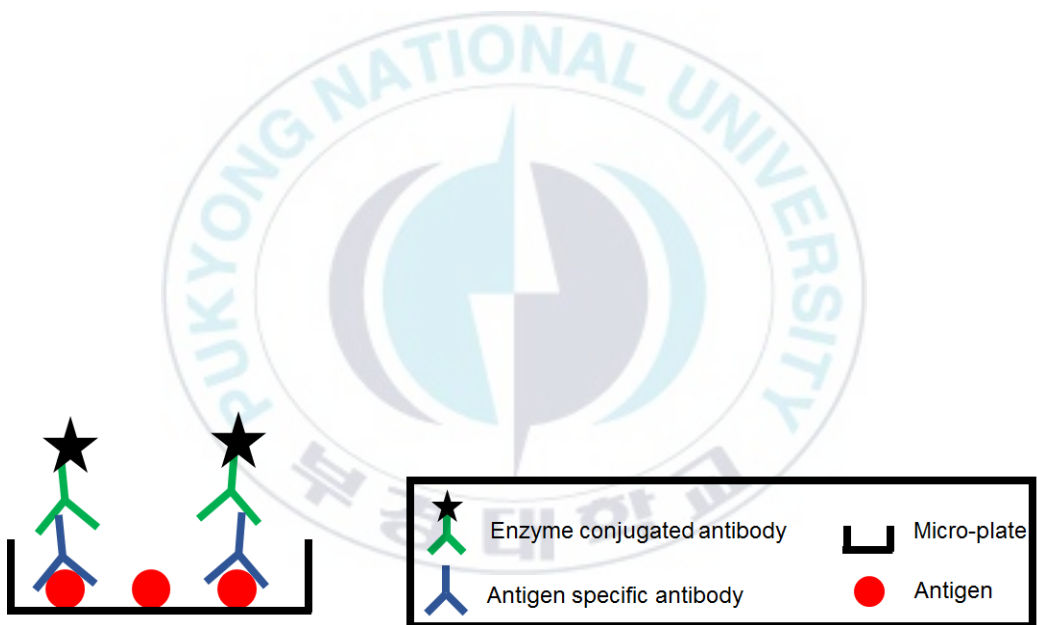


Figure 2. Indirect ELISA method.

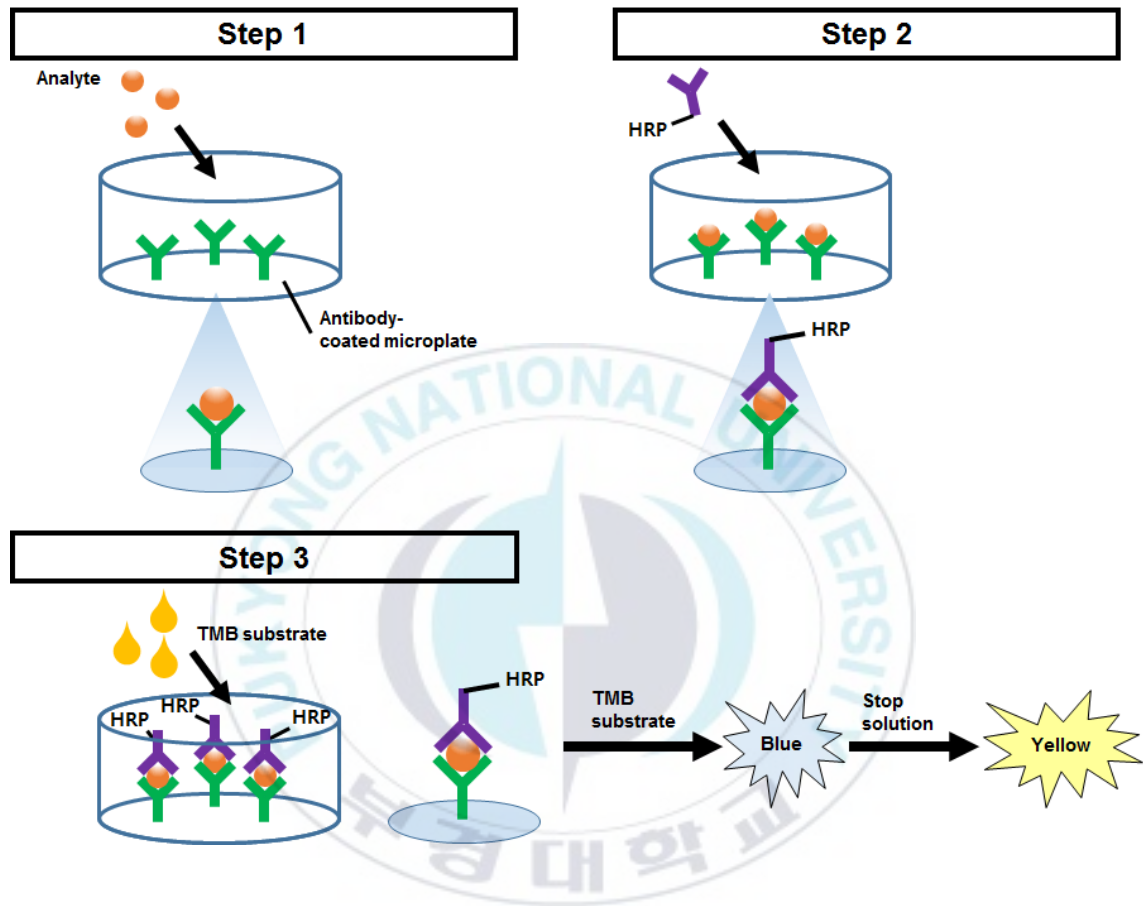


Figure 3. Sandwich ELISA method.

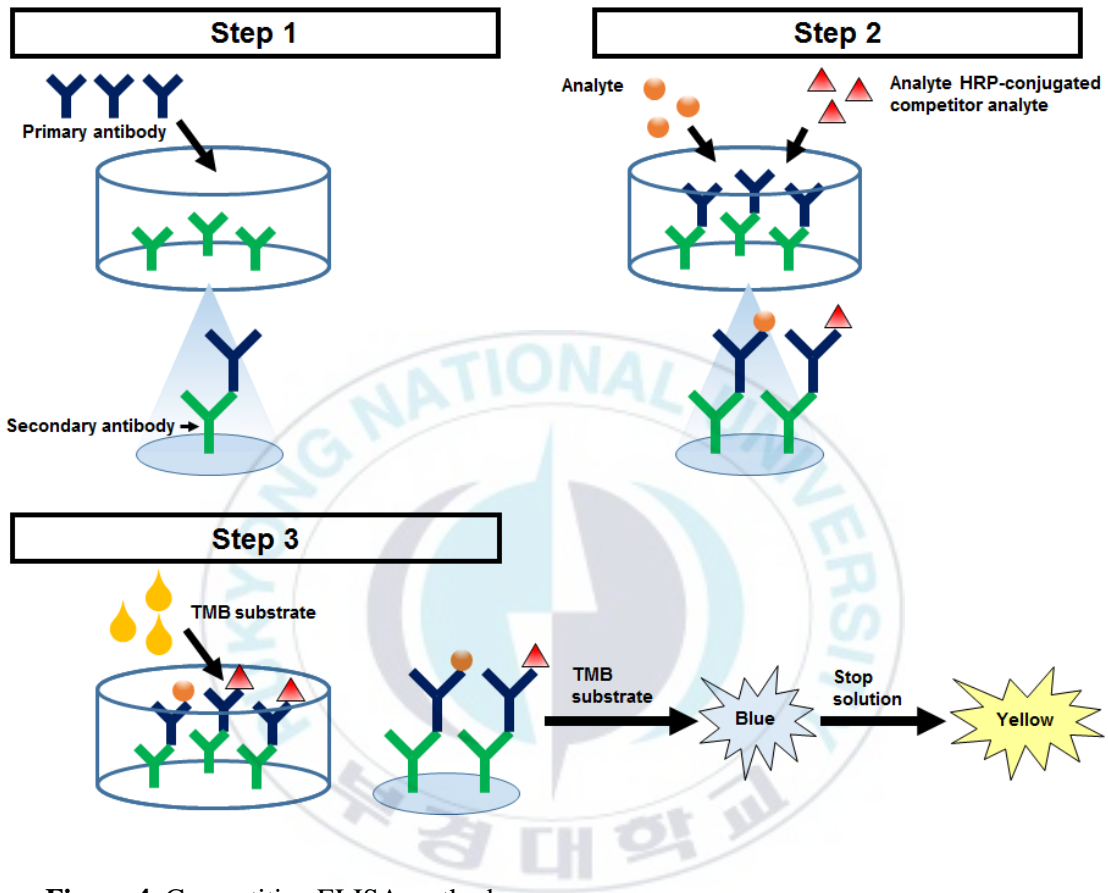


Figure 4. Competitive ELISA method.

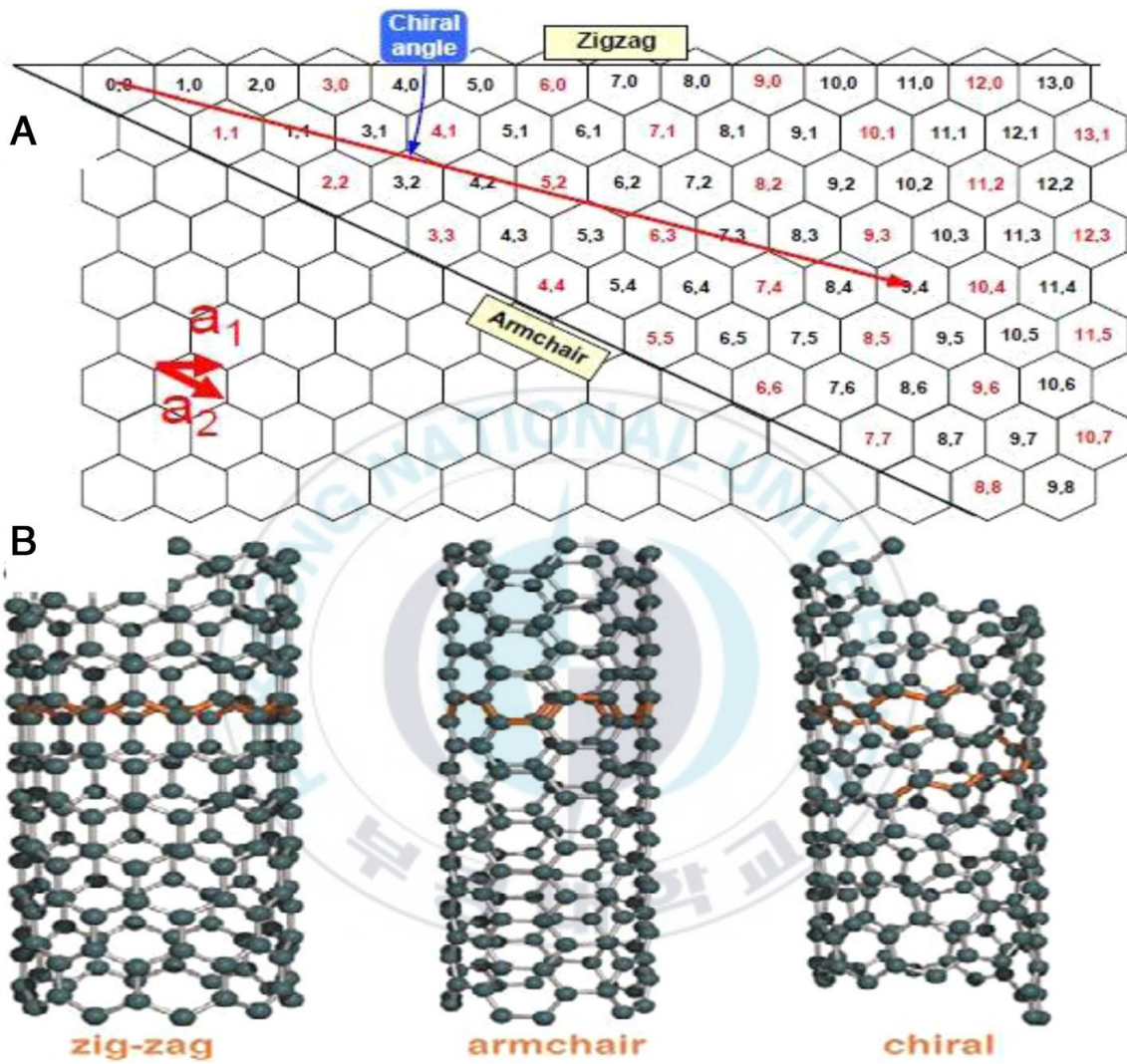


Figure 5. Different forms of SWCNTs. (A) The chiral vector C also determines the tube diameter. (B) Models of three atomically perfect SWCNT structures.²¹

2. Experimental section

2.1 Chemicals and materials

Nitric acid (64.0~66.0%) was purchased from DUKSAN Science. Phosphate buffered saline (PBS, pH = 7.2) was purchased from Biosesang Inc. 1 M 2-(N-morpholino)ethanesulfonic acid (MES, pH = 5.0) and 0.05% Tween 20 + 1% bovine serum albumin (BSA) in PBS were purchased from Tech & Innovation. N-(3-Dimethylaminopropyl)-N'-ethylcarbodiimide hydrochloride (EDC), N-Hydroxysulfosuccinimide sodium salt (NHSS), monoclonal anti-KLK3 antibody produced in mouse (PSA antibody, species reactivity is human) and prostate specific antigen from human semen (PSA) were purchased from Sigma-Aldrich. Micro-pore filter paper (mixed cellulose ester, diameter 25 mm, pore size 0.45 μm) was purchased from Toyo Roshi Kaisha, Ltd. Syringe (10 mL) was purchased from Korea Vaccine Co., Ltd. Silver paste (Dottite) was purchased from Fujikura Kasei Co., Ltd. Hydrochloric acid (35.0~37.0%) was purchased from SAMCHUN PURE CHEMICAL Co., Ltd. 2-Aminoethanethiol hydrochloride (98%), gold(III) chloride trihydrate ($\geq 99.9\%$ trace metals basis), sodium citrate dihydrate (99%), sodium borohydride ($\geq 98.0\%$) and thioglycolic acid ($\geq 99\%$) were purchased from Sigma-Aldrich. Multi-wall carbon nanotubes (MWCNTs, diameter 20 nm, length 5 μm) were purchased from Carbon Nano-material Technology Co. MWCNTs were produced by chemical vapor deposition (CVD) using iron and molybdenum catalyst. Human Kallikrein 3/PSA ELISA kit (96-well) was purchased from Ab Frontier.

2.2 Fabrication of biosensor based on carboxylated MWCNTs

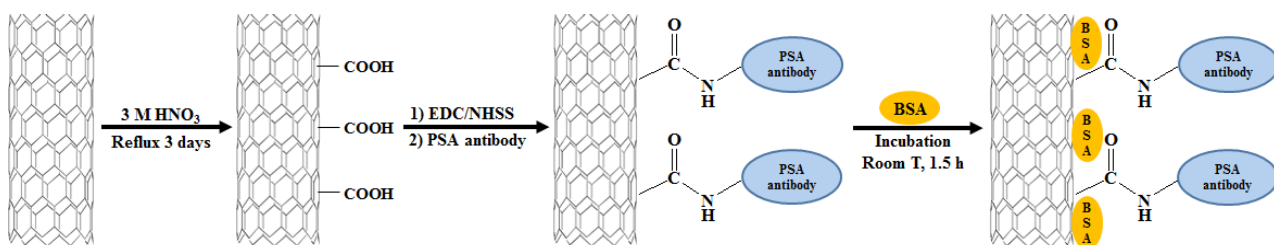
MWCNTs (300 mg) were refluxed in 20 mL of 3.0 M nitric acid at 105 °C for 3 days to generate carboxyl group on the MWCNTs.⁴⁵ The functionalized MWCNTs solution was washed and filtered more than 10 times with distilled water until pH was ~7. The carboxylated MWCNTs were dried at 100 °C for 24 h in oven. The carboxyl groups on the surface of MWCNTs were confirmed by Fourier transform infrared spectrometer (FT-IR, JASCO FT/IR-4100). The first step in Scheme 1 is this carboxylation process.

The carbonyl groups on MWCNTs can accommodate PSA antibody by following steps.³⁶ The carboxylated MWCNTs (1.3 mg) were dispersed in 0.1 M MES buffer 4 mL with 0.4 mmol mM EDC and 0.1 mmol NHSS. This dispersion was sonicated in a sonicator (Jeio Tech, UC-02) for 1 min and mixed with a vortex mixer (Scientific industries, Inc.) at room temperature for 15 min. The resulting mixture was centrifuged (Hanil Science Industrial Co.,Ltd., HA-1000-3) with 3000 rpm for 10 min, and the supernatant was discarded. At least 5 times washing with PBS was performed to remove excessive EDC and NHSS from the precipitation. The PSA antibody 0.5 mL (0.01 mg/mL) was added to the mixture and stirred in a vial for overnight at room temperature to attach on MWCNTs. This procedure is shown at second step in Scheme 1.

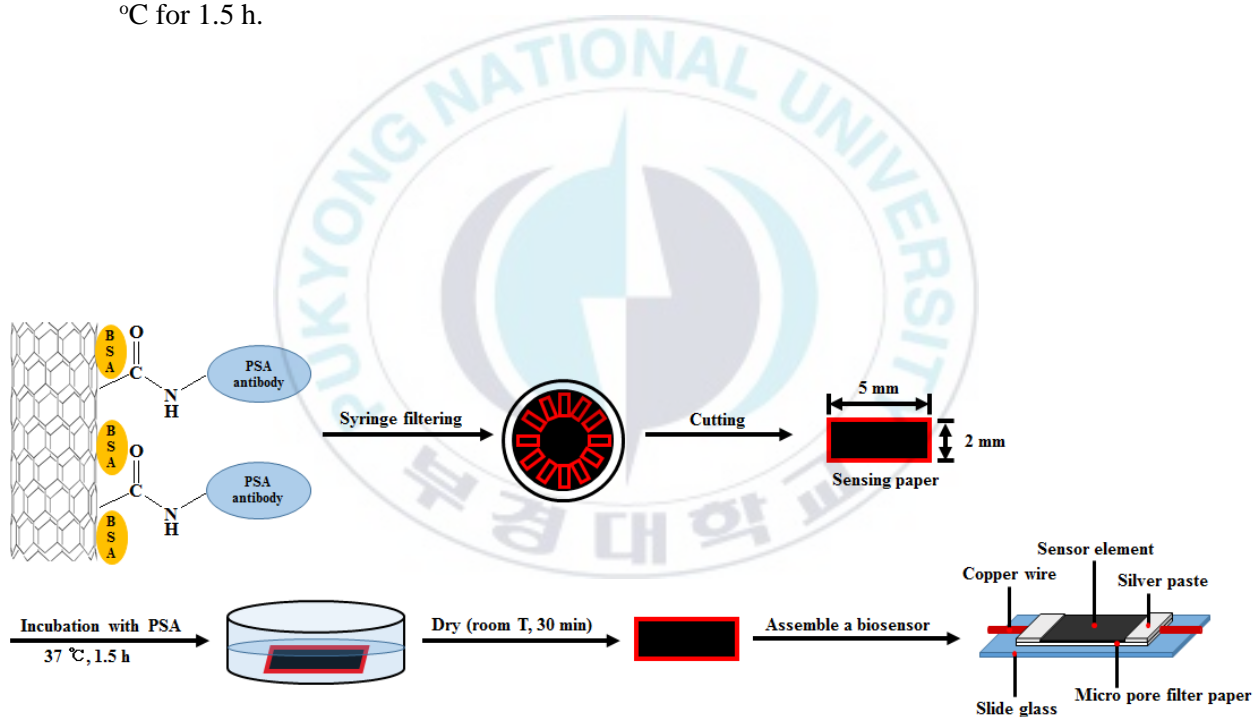
The final stage to prepare the MWCNTs based biosensor is prevention of unwanted interaction between PSA antibody attached MWCNTs and target PSA; a mixed solution of 0.05% Tween 20 in 1% BSA (100 µL) was added into the above PSA antibody added mixture (2 mL) to avoid attachment of PSA on the surface of MWCNTs. The BSA inhibits non-specific binding of PSA with the sensor element^{46,47} and Tween

20 cleans the binding site of PSA antibody.³⁶ The mixture was incubated at room temperature for 1.5 h. The resulting mixture was centrifuged at 3000 rpm for 5 min, and supernatant was removed. The precipitate was washed and centrifuged with PBS buffer 5 times to remove any free PSA antibody and BSA. This procedure is shown at third step in Scheme 1. The prepared sample by this stage named as Ab-MWCNTs, which stands for PSA antibody attached on MWCNTs.

The Ab-MWCNTs were deposited on a micro-pore filter paper by the syringe filtering. This stage is the first step in Scheme 2. The Ab-MWCNTs deposited on the micro-pore filter paper should not be dried until completion of the sensing to maintain activity of antibody. This Ab-MWCNTs deposited filter paper was cut into $5 \times 2 \text{ mm}^2$ size sensor elements from the center to the circumference of the filter paper. This cutting method was very important to keep the uniform resistance for all sensor elements. A drop (100 μL) of PAS contained solution (0 ~ 1000 ng/mL) was loaded on top of the sensor element. Again, it should be stressed that the samples should not be dried to keep the bioactivity of the all proteins. Then the sensor element was incubated at 37 °C for 1.5 h and dried in air at room temperature for more than 30 min. The resistance of the incubated sensor was measured by using a digital multimeter (Hewlett-Packard Co. multimeter 3478A or Agilent 34401) at the ambient condition. A silver paste was used to keep the electrical contacts between the sensor element and copper wires. Basic morphological information of materials was observed with an atomic force microscope (AFM, Park scientific instruments) and a scanning electron microscope (SEM, HITACHI S-2400).



Scheme 1. Preparation of the activated MWCNTs with PSA antibody. Incubated at 37 °C for 1.5 h.



Scheme 2. Preparation of sensor element and PSA detection procedure.

2.3 Fabrication of biosensor based on Au-MWCNTs

The carboxylation of MWCNTs was performed to generate carboxyl group. To increase the number of carboxyl group on the wall of MWCNTs more strong acid was used for the carboxylation process.

In order to remove the catalyst of commercial MWCNTs, the MWCNTs (200 mg) were added to 75 mL of concentrated (36%) hydrochloric acid and mixture was stirred at room temperature for 5 h. The resulting mixture was filtered and washed with distilled water until pH was ~7. The pristine MWCNTs were dried at 80 °C for 12 h in oven. (The catalyst removal is option. Because the catalyst of MWCNTs could be removed by nitric acid reflux for carboxylation of MWCNTs.) The pristine MWCNTs (150 mg) were refluxed in 15 mL of 14 M nitric acid at 105 °C for 3 days to generate carboxyl group on the MWCNTs. The functionalized MWCNTs solution was filtered and washed with distilled water until pH was ~7. The carboxylated MWCNTs were dried at 100 °C for 24 h in oven. This procedure is shown at first step in Scheme 3.

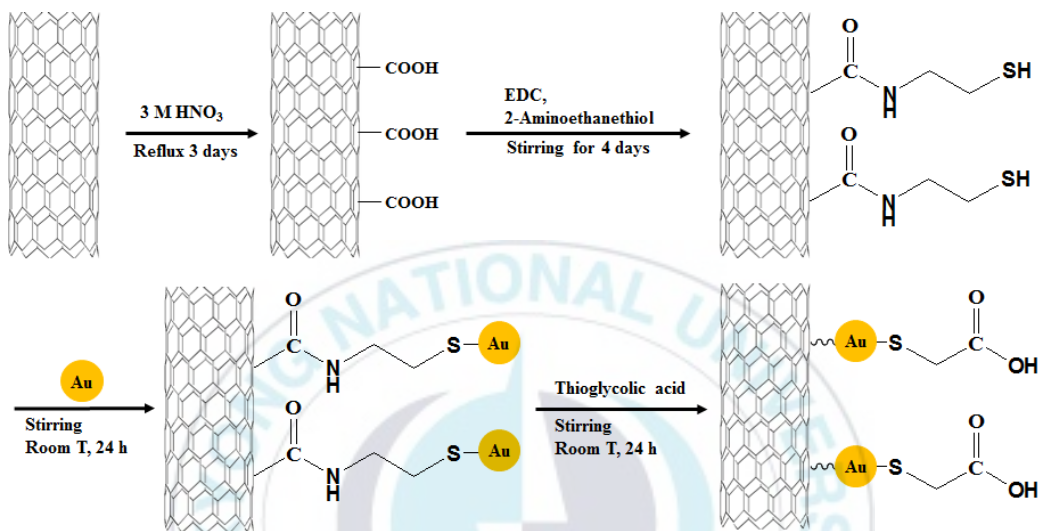
The thiolation of the carboxylated MWCNTs was conducted to attach gold nanoparticles (Au NPs) on the surface of MWCNTs.⁴⁸ Au NPs and thiol group form a strong bond.⁴⁹ Carboxylated MWCNTs (50 mg), EDC 10 mmol and 2-aminoethanethiol hydrochloride 40 mmol were mixed in 0.1 M MES buffer 100 mL. The mixture was vigorously stirred at room temperature for 4 days. The resulting mixture was filtered and washed more than 5 times and dried at 80 °C for 24 h in oven. The prepared thiolated MWCNTs were characterized by FT-IR. This procedure is shown at second step in Scheme 3.

The gold nanoparticles (Au NPs) were prepared as follows. A 200 mL aqueous solution containing 1 mM HAuCl₄ and 3 mM sodium citrate was prepared in a conical

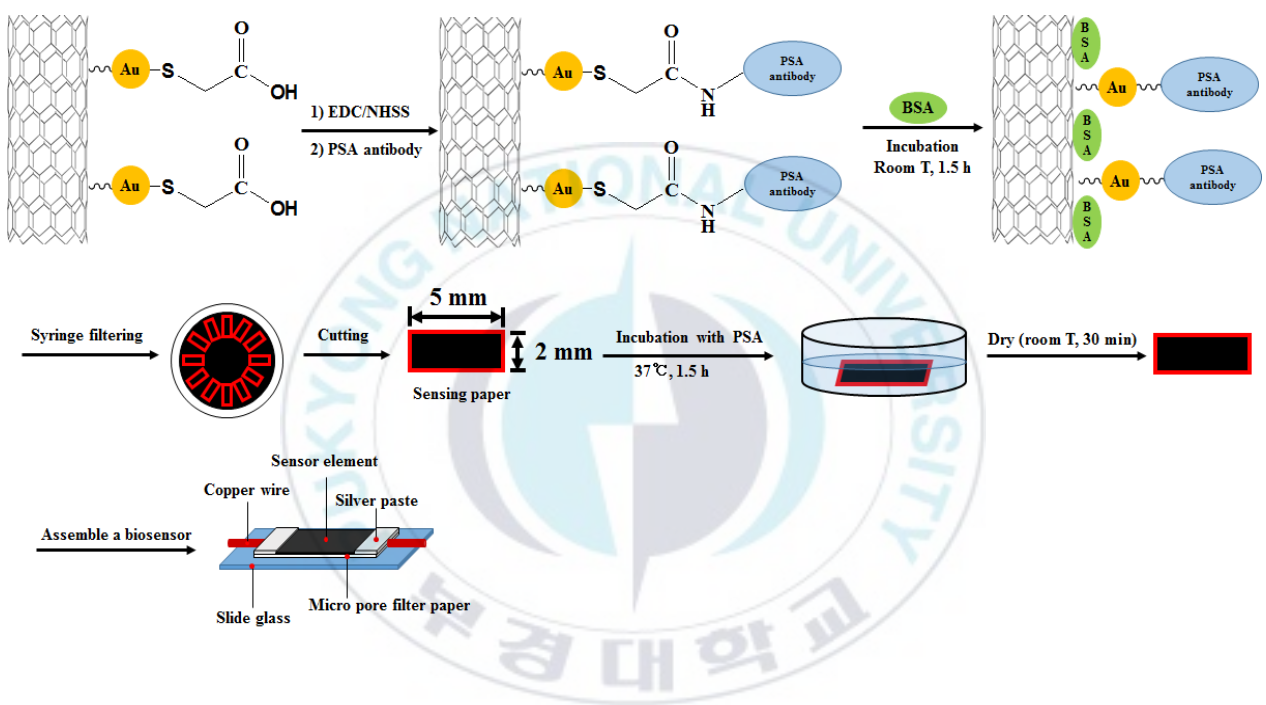
flask. Next, 1 mL of ice cold 0.6 M NaBH₄ solution was added to the solution all at once while vigorous stirring. The color of solution turned dark purple immediately after adding NaBH₄, indicating the formation of Au NPs. The prepared Au NPs were promptly used and characterized by TEM and UV-Vis spectrometer (Varian Cary 1C, Agilent Technologies).

The thiolated MWCNTs (40 mg) were added to 200 mL of prepared Au NPs solution. The mixture was sonicated for 1 h in ice bath and then vigorously stirred at room temperature for 24 h. The resulting solution was filtered and washed 5 times with distilled water to remove excessive Au NPs. This procedure is shown at third step in Scheme 3. The Au NPs attached MWCNTs were added to 10 mM thioglycolic acid 200 mL in order to attach PSA antibody on the surface of Au NPs. Then mixture was stirred at room temperature for 24 h. The resulting solution was filtered and washed more than 5 times to remove excessive thioglycolic acid. The functionalized MWCNTs were dried at 110 °C for 24 h in oven. At this step, Au NPs attached MWCNTs will be named Au-MWCNTs. The Au-MWCNTs were characterized by TEM. This procedure is shown at fourth step in Scheme 3.

Next experimental procedures that include antibody attachment, BSA block, fabrication of biosensor and PSA detection as shown in Scheme 4 are the same as previously introduced method that is 2.2 Fabrication of biosensor based on carboxylated MWCNTs.



Scheme 3. Preparation of gold nanoparticles attached MWCNTs for fabrication of PSA detectable sensor element.



Scheme 4. PSA detection process and biosensor assembly.

2.4 Commercial ELISA kit performance test

The human kallikrein 3 standard solutions (concentration is 10, 5, 2.5, 1.25, 0.625, 0.312, 0.156 and 0 ng/mL) 100 μ L are located into the precoated 96-well plate respectively. Then, plate was incubated at 37 °C for 1.5 h. Plate contents were discarded without washing, and biotinylated antibodies (diluted in 1:99 by antibody dilution buffer) 100 μ L were added into plate. Plate was incubated at 37 °C for 1 h, then plate was carefully washed 3 times with 1 \times PBS. Avidin-biotin-peroxidase complex (ABC, diluted in 1:99 by ABS dilution buffer) working solution 100 μ L was added into plate and was incubated at 37 °C for 30 min. Incubated plate was carefully washed 5 times with PBS. Then 3,3',5,5'-Tetramethylbenzidine (TMB color developing agent) 90 μ L was added into plate and was incubated at 37 °C in dark for 30 min (blue color will be appeared), and TMB stop solution 100 μ L was added into plate (blue color will be promptly changed to yellow color). The optical density (O.D.) absorbance of solution in the plate was measured at 450 nm by microplate reader (Pharm Tek Systems, FilterMax F5 Multi-Mode Microplate Reader) within 30 min after adding the stop solution.

The ABC working solution and TMB color developing agent were kept warm at 37 °C for 30 min before use. When diluting samples and reagents, they were mixed completely.

3. Results and discussion

3.1 Fabrication of biosensor based on carboxylated MWCNTs

Generally, sulfuric acid/nitric acid (without dilution, 3:1 volume, respectively) treatment was selected for carboxylation of CNTs.⁵⁰ The CNTs were cut into small fragments to give low conductivity, and recovery of CNTs from the mixture was very hard. Therefore, we carboxylated the CNTs by using 3 M HNO₃.

Figure 6 shows IR spectra of the MWCNTs, carboxylated MWCNTs for 3 days in 3 M nitric acid and Ab-MWCNTs. It is clear that the peak position corresponding to the carbon-carbon double bond of MWCNTs is 1630 cm⁻¹. And the peak at 1715 cm⁻¹ corresponds to the C=O bond of the carboxyl group, which generated by the nitric acid treatment of MWCNTs. The presence of the carboxyl group results the reaction with the PSA antibody. The carboxyl group at the surface of MWCNTs can react with amine group of L-lysine unit in PSA antibody.⁵¹ This is a simple substitution reaction to form amide group. Before the reaction, the carboxylated MWCNTs were treated with EDC/NHSS to induce a substitution reaction between the hydroxyl group in carboxyl group and amine group in PSA antibody. The IR spectrum of this Ab-MWCNTs is blue line in Figure 6. The spectrum shows emerge of the complex amide band nearly at 1550 cm⁻¹.

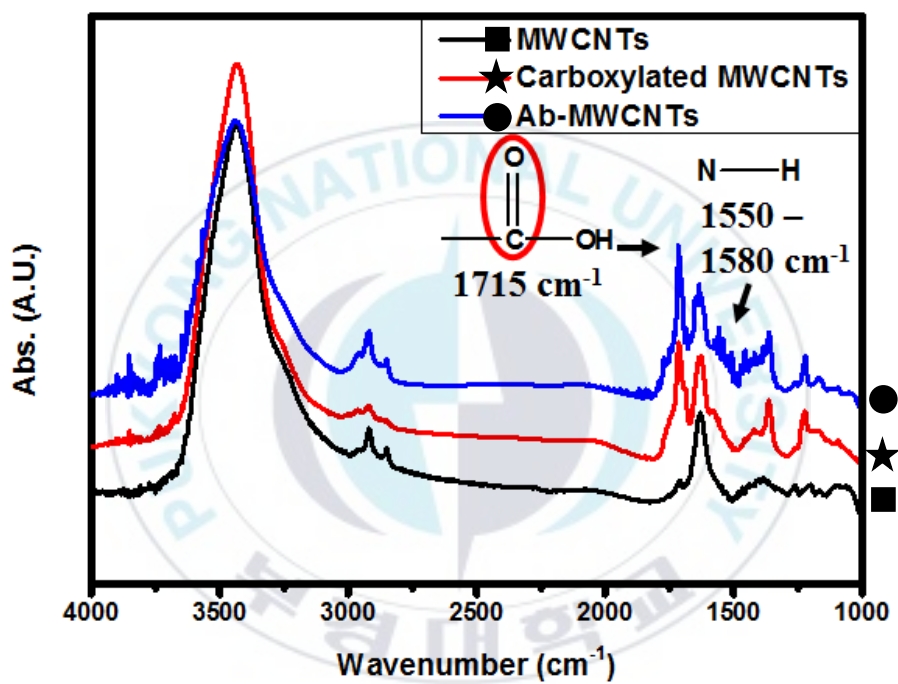


Figure 6. FT-IR spectra of MWCNTs, carboxylated MWCNTs and Ab-MWCNTs.

Figure 7 is SEM and AFM images of the MWCNT based elements. The samples were deposited on a filter paper without the BSA block process and then dried at ambient condition for more than 2 h. Figure 7(a) and (b) show SEM and AFM images of carboxylated MWCNTs. The observed diameter of MWCNTs in both images is about 20 nm. That corresponds to the diameter of the as received MWCNTs. There wasn't observable damage on the surface of carboxylated MWCNTs. All the MWCNTs could be distinguished in both images. Figure 7(c) and (d) are SEM and AFM images of Ab-MWCNTs. The observed diameter of the antibody attached MWCNTs seems the same as that of carboxylated MWCNTs. Any irregularly attached object wasn't observed on the tube surface. This indicates the attachment of the antibody may be not the wrap-coating on the whole surface of the MWCNTs. We believe that the cotton ball like areas in the SEM image is the result of the increased interaction between the attached antibody and the MWCNTs. In this area, the MWCNTs might be inserted into the antibody. Figure 7(e) and (f) are SEM and AFM images of PSA-Ab-MWCNTs. In the SEM image, most of the MWCNTs are covered with the proteins (PSA antibody and PSA). The cotton ball like parts spread over the whole surface of the deposited film. The shape of cotton ball like parts is not clearly observed in AFM images due to the softness of proteins. The optically observed compactness of the deposit film was in order carboxylated MWCNTs \geq Ab-MWCNTs $>$ PSA-Ab-MWCNTs. The root mean square (RMS) roughness of the surface of the film is in the same order with the eye observation; 38, 32 and 61 nm for carboxylated MWCNTs, Ab-MWCNTs and PSA-Ab-MWCNTs, respectively.

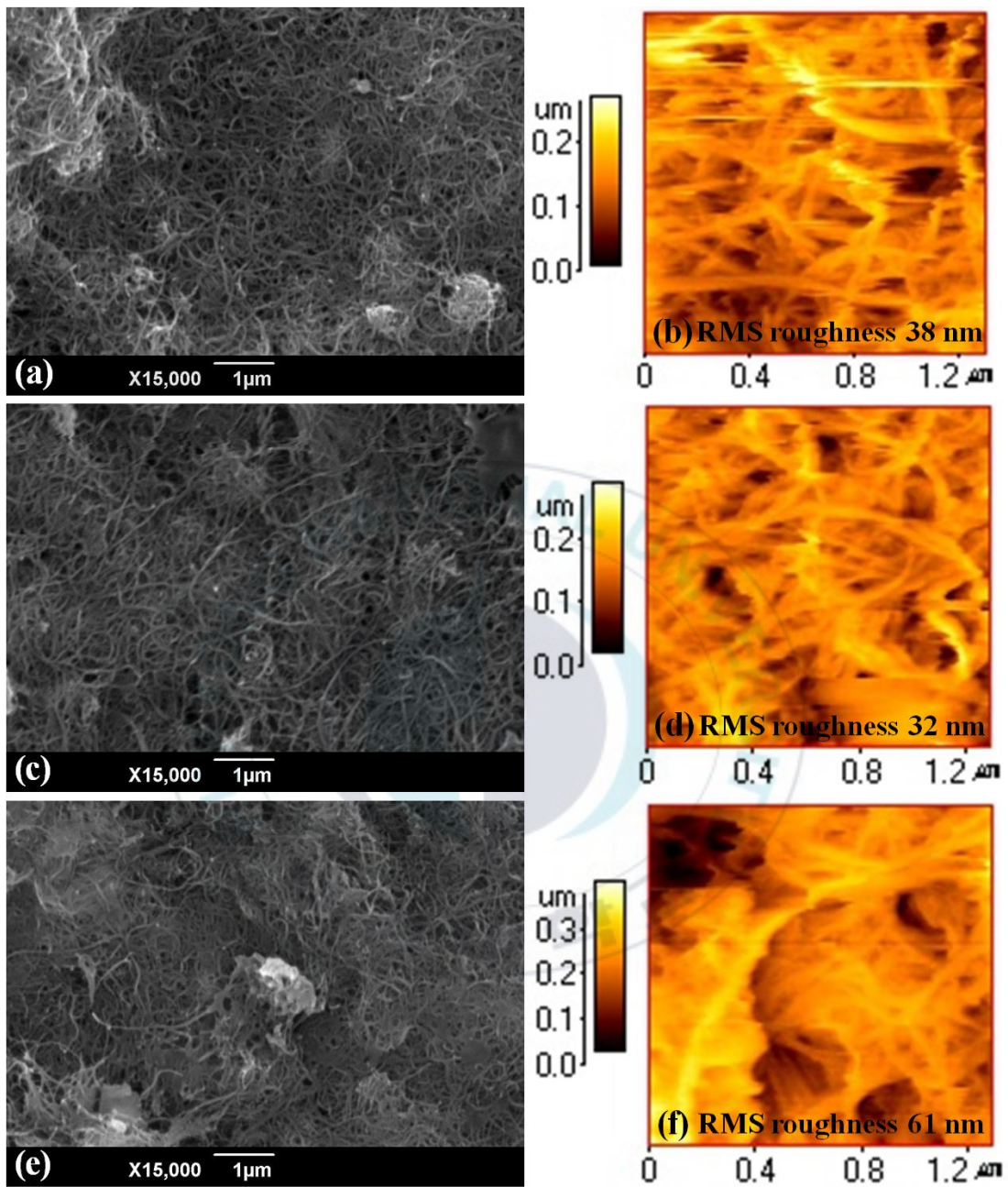
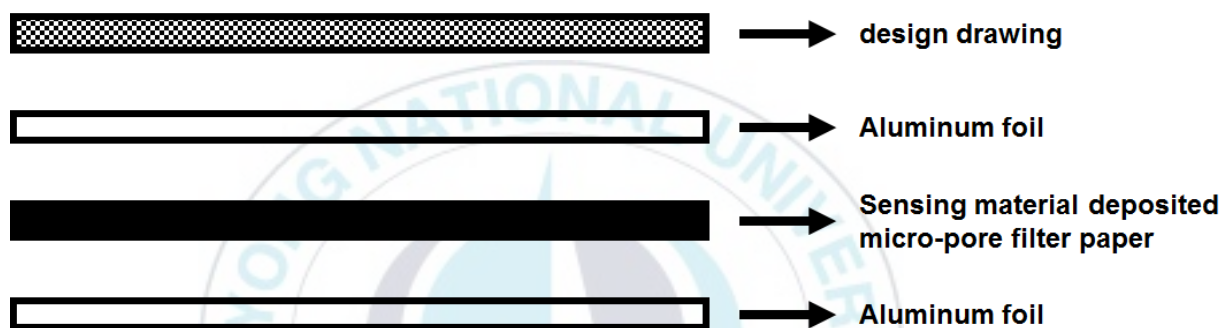


Figure 7. (a) is SEM image, and (b) is AFM image of carboxylated MWCNTs. (c) is SEM image, and (d) is AFM image of Ab-MWCNTs. (e) is SEM image, and (f) is AFM image of PSA-Ab-MWCNTs. Scanned area for the AFM images was $2.0 \times 2.0 \mu\text{m}^2$.

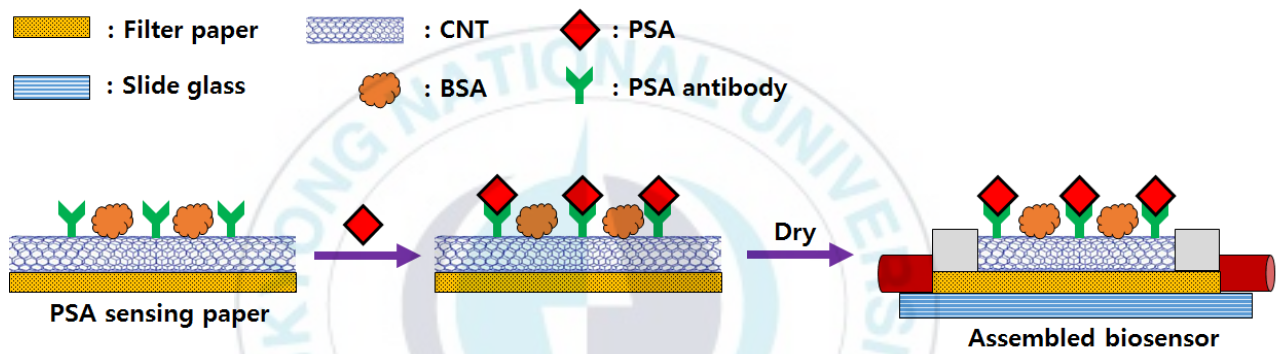
The prepared sensing paper (Ab-MWCNTs), which is BSA blocked Ab-MWCNTs deposit micro-pore filter paper, should be wet until the end of the site specific reaction between PSA antibody and PSA. The cutting procedure shown in Scheme 5 ensure the exact size ($5 \times 2 \text{ mm}^2$) of sensing paper and preservation of wet condition. The site specific reaction was accomplished by the incubation at $37 \text{ }^\circ\text{C}$ for 1.5 h. Subsequently sensing paper was dried and assembled to the biosensor shape and then performed the measurement of electrical resistance (Scheme 6). The measured resistance of a biosensor was compared to the background resistance of a sensor, which incubated Ab-MWCNTs with 0 ng/mL of PSA. The measured resistances of sensors were normalized with the dimensions of the sensor. The thickness of the sensor element was not considered, because we compared all values with the background value and the origin of the all sensor elements is the same batch. The most important factor in this sensing method is the uniformity of the MWCNTs layer, which deposited on a micro-pore filter paper, to keep constant value of the base resistance of the sensor element. The thickness of the sensor elements should be same. The uniformity can be achieved by the adjustment of the concentration level of the MWCNTs in the solution to $6.5 \text{ }\mu\text{g/mL}$. The infiltrated volume of the Ab-MWCNTs solution was 200 mL . As Figure 8, the thickness of the deposited Ab-MWCNTs layer was confirmed to be about $4.5 \text{ }\mu\text{m}$ by surface profiler (alpha step-500, Tencor, USA). In order to obtain Ab-MWCNTs layer without filter paper, filter paper in Ab-MWCNTs deposited filter paper was removed by acetone. The Ab-MWCNTs layer was loaded on slide glass and surface of Ab-MWCNTs was cut by knife for precise measurement. The cutting method of sensor element, cut from center to circle, is most important to keep the uniform resistivity. Deposited MWCNTs layer that has the most uniform thickness was obtained when MWCNTs deposited filter paper was cut into sunflower shape as Figure 9(a). When

filter paper was cut as Figure 9(a) and (b), standard deviation of the relative electrical resistance for each sample was 0.03 and 0.05 respectively. In case of MWCNTs, deposited MWCNTs layer lack uniformity of the because of weak dispersion in aqueous solution. As expected, this type of detection of PSA has great advantages such as superior portability, time saving and cost cutting than well-known ELISA as mentioned.





Scheme 5. Strategy for cutting to exact size ($5 \times 2 \text{ mm}^2$) of sensing paper and preservation of sensing materials in wet.



Scheme 6. PSA detection process and assembly of biosensor.

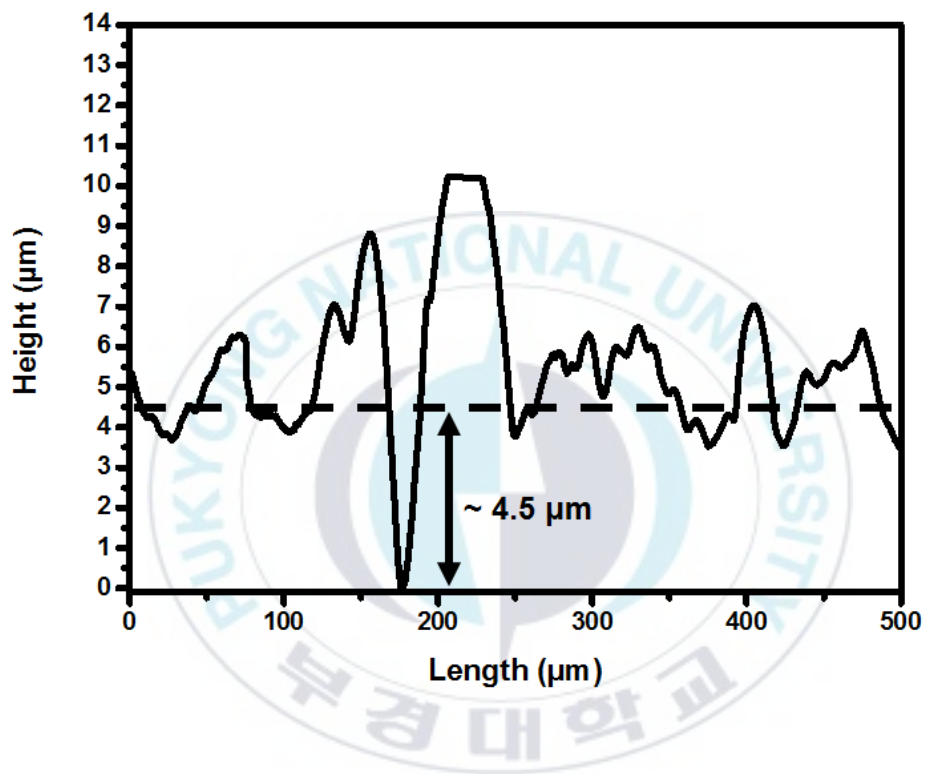


Figure 8. Height profile measured by alpha-step. Thickness of Ab-MWCNTs layer in sensing paper was measured after removing the filter paper.

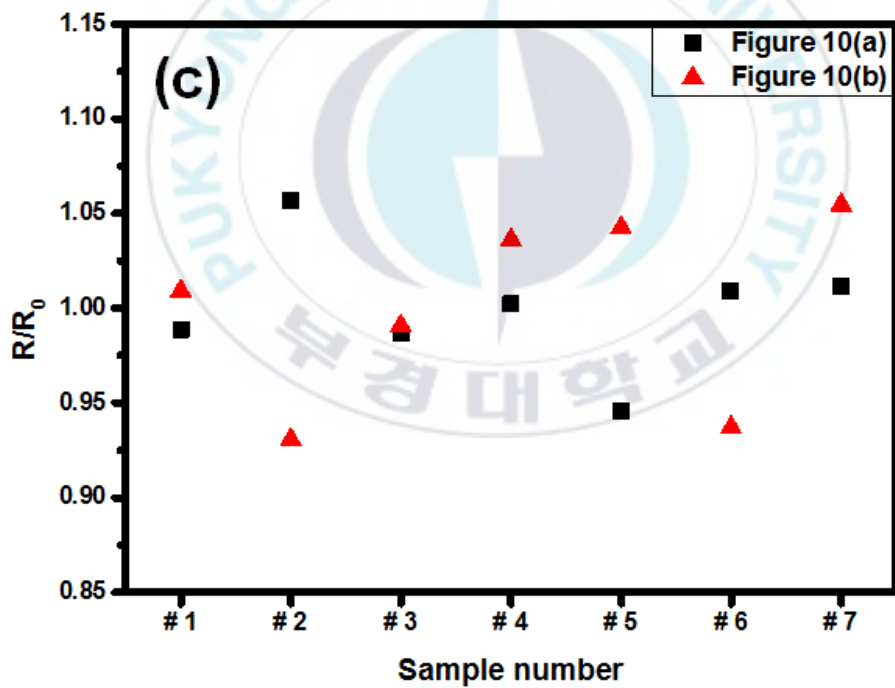
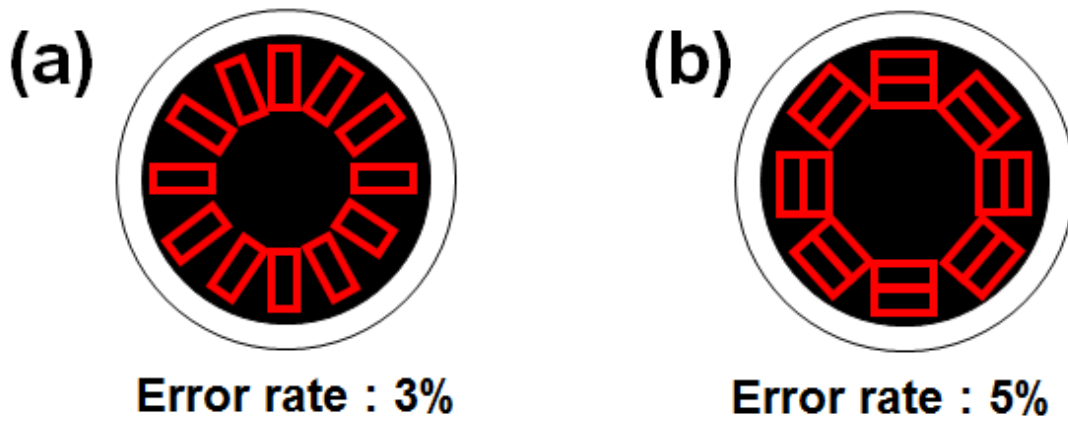


Figure 9. (a) and (b) show the ways to cut the sensing element. (c) Relative electrical resistance value for respective sample.

I-V curves of the MWCNTs, carboxylated MWCNTs, Ab-MWCNTs and PSA-Ab-MWCNTs are shown in Figure 10. All the MWCNTs obey the Ohm's law at high current range (from -1.4 mA to +1.4 mA) as well as low current range (from -1.0 μ A to +1.0 μ A). The more proteins attached to the MWCNTs the slope of I-V curves was increased. The electrical resistance of each MWCNTs could be estimated from the slope of the plot as list in the Table 1. The electrical resistance has increased to 500% by carboxylation of the MWCNTs. The decrement of sp^2 character in MWCNT during the carboxylation process will cause mainly this increment of resistance. The electrical resistance of Ab-MWCNTs, which is PAS antibody attached on the carbonyl group, is increased about 160% higher than that of carboxylated MWCNTs. We believe the increased resistance by the attachment of the additional protein (PSA-antibody) originated by the increased potential height between MWCNTs as discussed in the later section. By the same reason, PSA-Ab-MWCNTs (PSA, 1000 ng/mL) have 150% higher resistance than the Ab-MWCNTs. This increment clearly displayed in Figure 11.

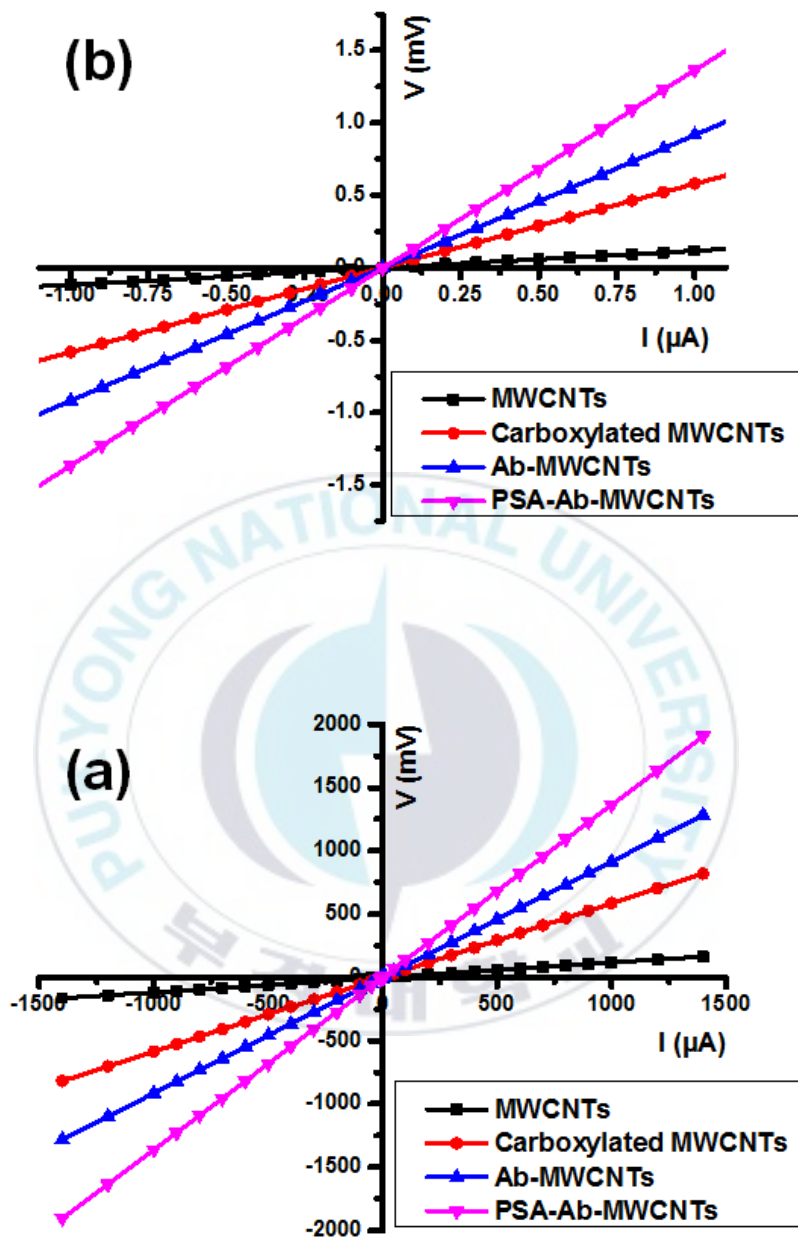


Figure 10. I-V curves for MWCNTs, activated MWCNTs with carboxyl group, Ab-MWCNTs and PSA-Ab-MWCNTs in the current range of ± 1.40 mA (a) and ± 1.00 μA (b).

	Initial amount of the MWCNTs (mg)	I-V curve slope	Resistance (Ω)	R/R_0
MWCNTs	1.16	0.117	117	1.00
Carboxylated MWCNTs	1.16	0.585	585	5.00
Ab-MWCNTs	1.30	0.916	916	7.81
PSA-Ab-MWCNTs	1.30	1.36	1360	11.6

Table 1. The relative resistances of MWCNTs, carboxylated MWCNTs, Ab-MWCNTs, and PSA-Ab-MWCNTs, those are estimated from the Figure 10.

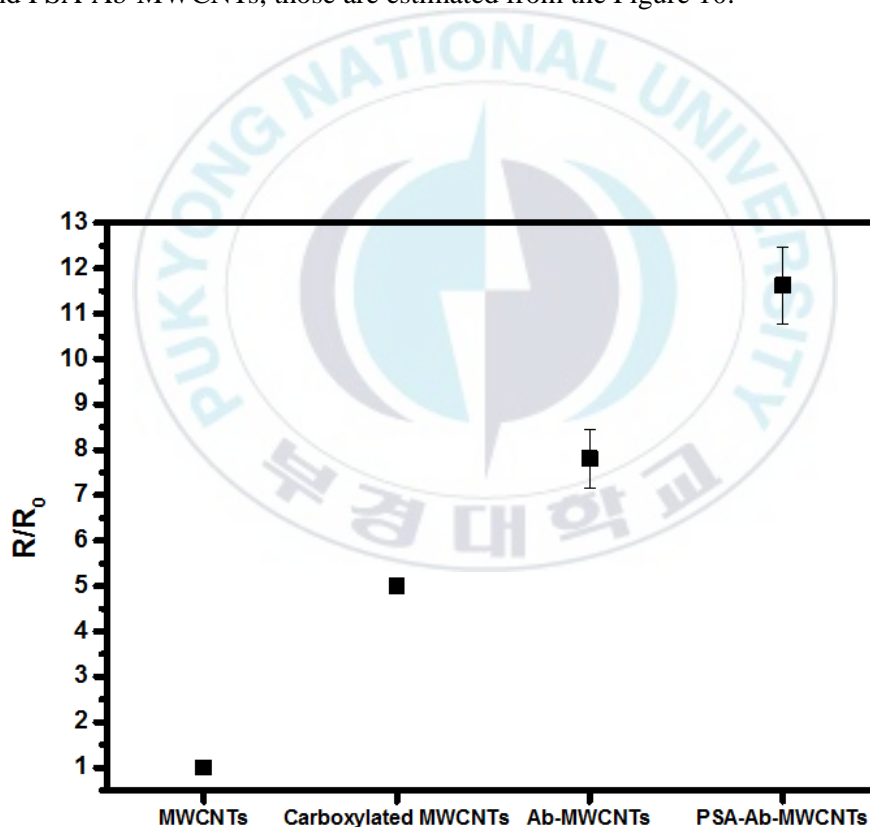


Figure 11. The electrical resistance of MWCNTs, carboxylated MWCNTs, Ab-MWCNTs and PSA-Ab-MWCNTs (PSA: 1000 ng/mL).

The change of the relative electrical resistance (R/R_0 : when R is resistance of the sensed element and R_0 is resistance of the zero level PAS sensed element) of sensor element (Ab-MWCNTs) by the reaction with PSA concentration is shown in Figure 12. Figure 12(a) shows that the change of relative resistance nearly linearly depends on the concentration of PSA in the range of 0 ~ 500 ng/mL. This indicates that the concentration of the PSA can be estimated by the electrical resistance measurement of the sensor elements in the range. If the concentration of PSA is > 500 ng/mL, however, the sensor may be useless. The resistance of the sensor element seems saturated higher than 500 ng/mL.

Figure 12(b) shows the change of relative resistance in the low PSA concentration range (0–10 ng/mL). In this range, the relative resistance linearly depends on the concentration of PSA. As shown in the plot the sensor can detect low enough level of PAS to find early stage of prostate cancer. If PSA level is higher than 4 ng/mL the prostate cancer could be in the early stage. The detection limit, which was estimated by $2 \times$ standard deviation from the signal mean of eleven biosensors detecting blank samples without the PSA, was 1.18 ng/mL. The electrical signal of blank samples is shown in Figure 13 and standard deviation was 3×10^{-3} .

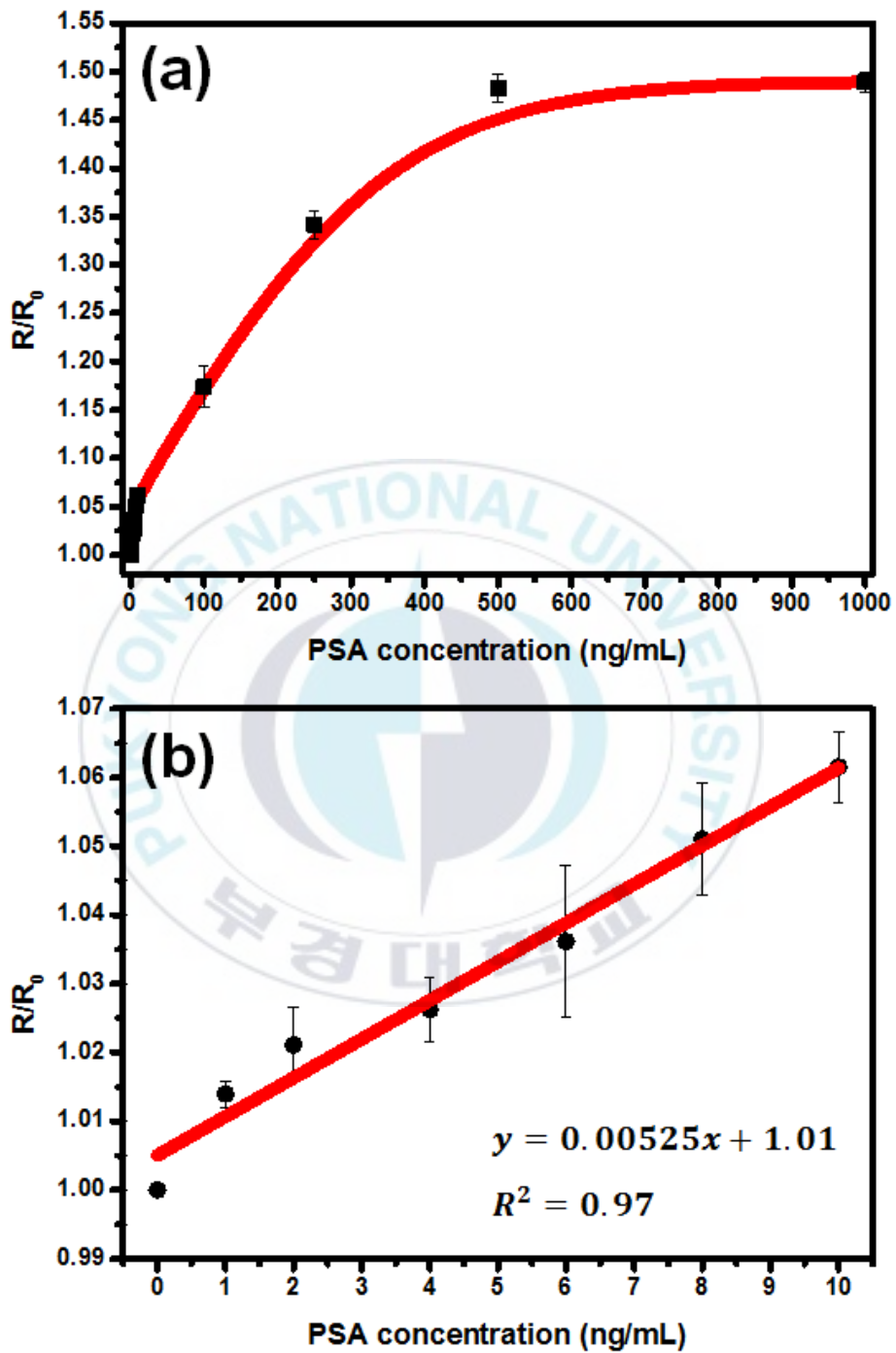


Figure 12. The plot of relative resistance vs. PSA concentration. For (a) wide range of PSA concentration (0-1000 ng/ml) and (b) low level of PAS (0-10 ng/mL).

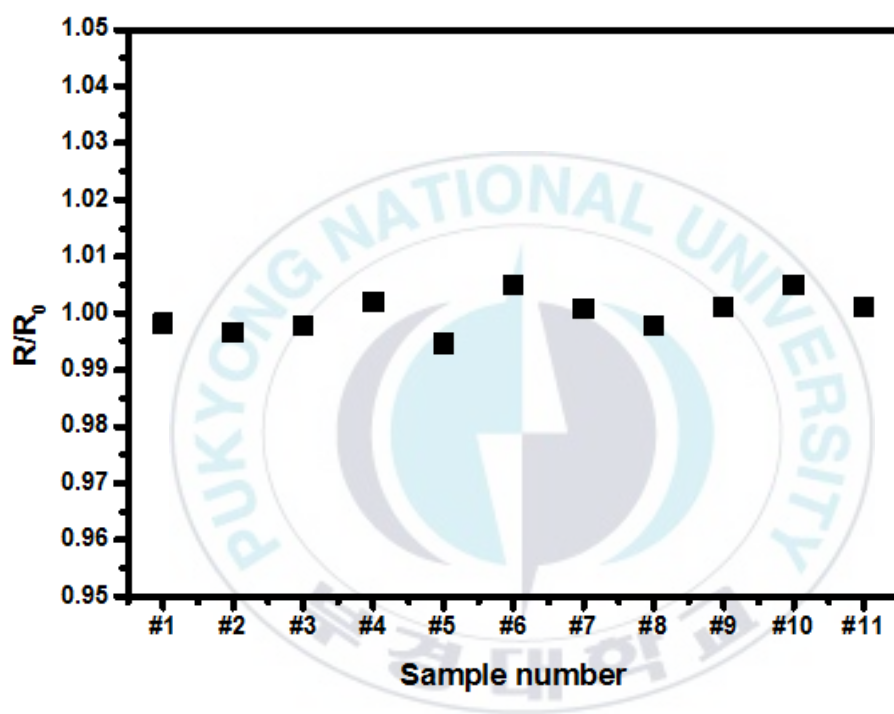


Figure 13. Electrical signal of background to determine the detection limit.

3.2 Fabrication of biosensor based on Au-MWCNTs

Figure 14(a) is TEM image of prepared Au NPs according to a published method by Nikhil R. Jana.⁵² The prepared Au NPs had a size distribution as shown in Figure 14(c) and the size of Au NPs was 3.6 nm. The color of Au NPs solution depends on the size of Au NPs by surface plasmon resonance.⁵³ The maximum absorbance of Au NPs solution was appeared at 513 nm as shown in Figure 15(a). As time passed, however the size of Au NPs was increased by the aging effect. The aging effect of Au NPs cause that absorbance peak has red shift. Figure 14(b) is TEM image of Au NPs 12 days later and Figure 14(d) shows size distribution of Au NPs. The size of aged Au NPs for 12 days was 4.6 nm. Also absorbance peak of Au NPs was red shifted from 513 nm to 517 nm. Therefore prepared Au NPs should be consumed as soon as possible and must be store at lightless condition and low temperature.

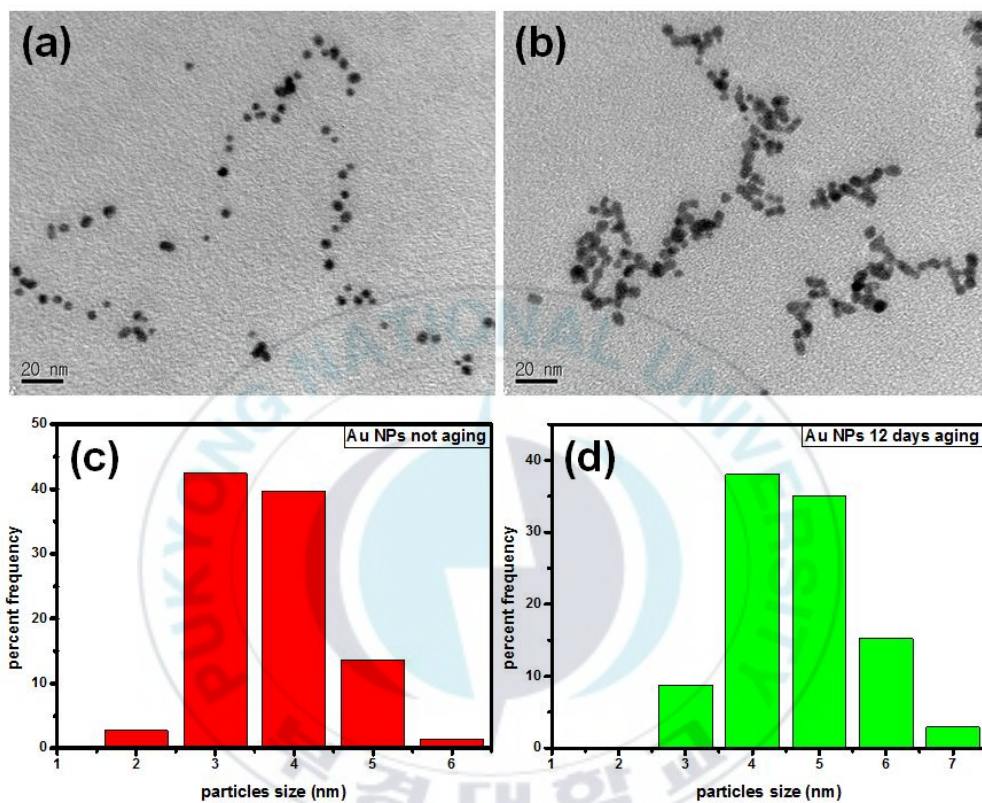


Figure 14. TEM image of the Au NPs and abundance ratio according to particles size. (a), (c) unaged Au NPs (size: 3.6 ± 0.7 nm) and (b), (d) aged Au NPs (size: 4.6 ± 0.9 nm) for 12 days.

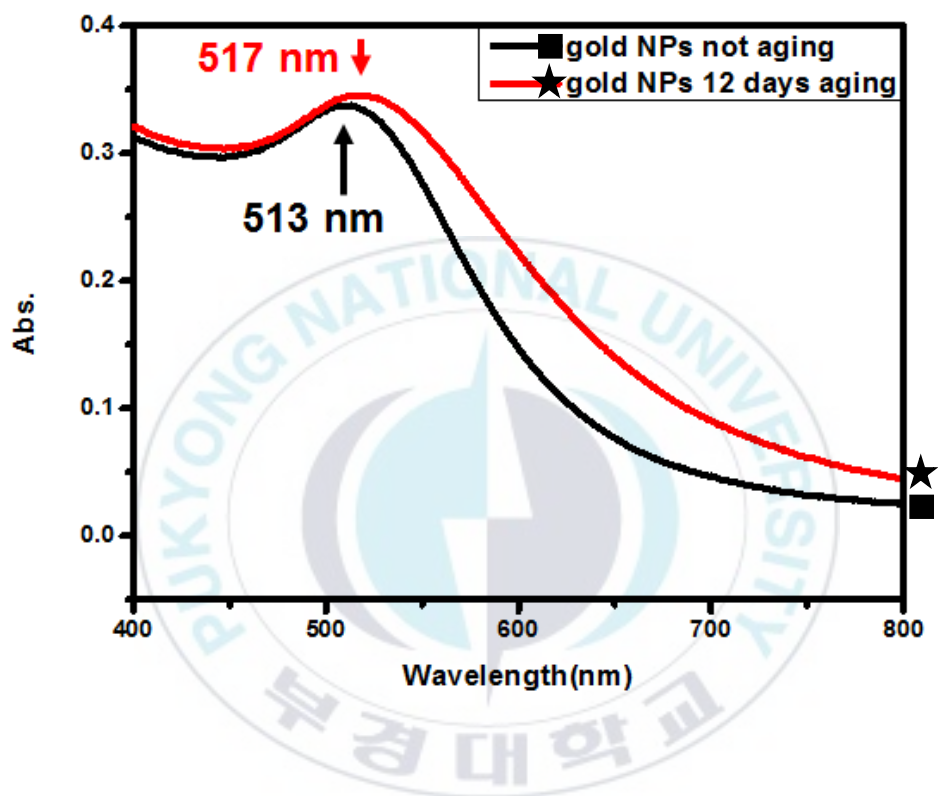


Figure 15. UV-Vis spectra of (a) Au NPs for unaged Au NPs and (b) 12 days aged Au NPs. The absorbance peak of unaged Au NPs became red shift by aging effect of Au NPs.

Figure 16 shows IR spectra of MWCNTs, carboxylated MWCNTs and thiolated MWCNTs. Thiolation of carboxylated MWCNTs is substitution reaction of hydroxyl group in carboxyl group with amine group in 2-aminoethanethiol which has amine group and thiol group. The characteristic peak of thiol group has peak position 2550-2620 cm^{-1} . However, the peak was not observed at here because of a small quantity of thiol group which was attached at the surface of chemically stable MWCNTs. Some peaks grew near at 1560 cm^{-1} by existence of N-H bond in amide group which was formed by reaction between carboxylated MWCNT and 2-aminoethanethiol by EDC/NHSS.

The Figure 17(a) and (b) are TEM image of Au-MWCNTs based on carboxylated MWCNTs and thiolated MWCNTs respectively when mixture of HAuCl_4 and functionalized MWCNTs was reduced simultaneously. Even though the Au NPs size shown in Figure 14 was 3.6 nm, the size of Au NPs attached at the carboxylated MWCNTs and thiolated MWCNTs was approximately 24 nm. Enlarged the size of Au NPs attached on the surface of functionalized MWCNTs was due to higher denseness of HAuCl_4 ions caused from interaction between functional group ($-\text{COOH}$ and $-\text{SH}$) of MWCNTs and HAuCl_4 .

Figure 18 is TEM image of Au-MWCNTs prepared by stirring the mixture of Au NPs (3.6 nm in diameter) and carboxylated MWCNTs (Figure 18(a)) or thiolated MWCNTs (Figure 18(b)). The Au NPs were not attached almost on the surface of carboxylated MWCNTs due to the weak interaction between carboxyl group and Au NPs. However, many Au NPs were attached on the thiolated MWCNTs as shown in Figure 17(b). Also the size of Au NPs was same to size of initially prepared Au NPs as shown in Figure 14(a). The Au NPs were observed in Figure 17(a), but Au NPs was nonexistent in Figure 18(a). The reason is due to not Au NPs attached to carboxyl group

of carboxylated MWCNTs by SA but produced the Au NPs including the wall of carboxylated MWCNTs.



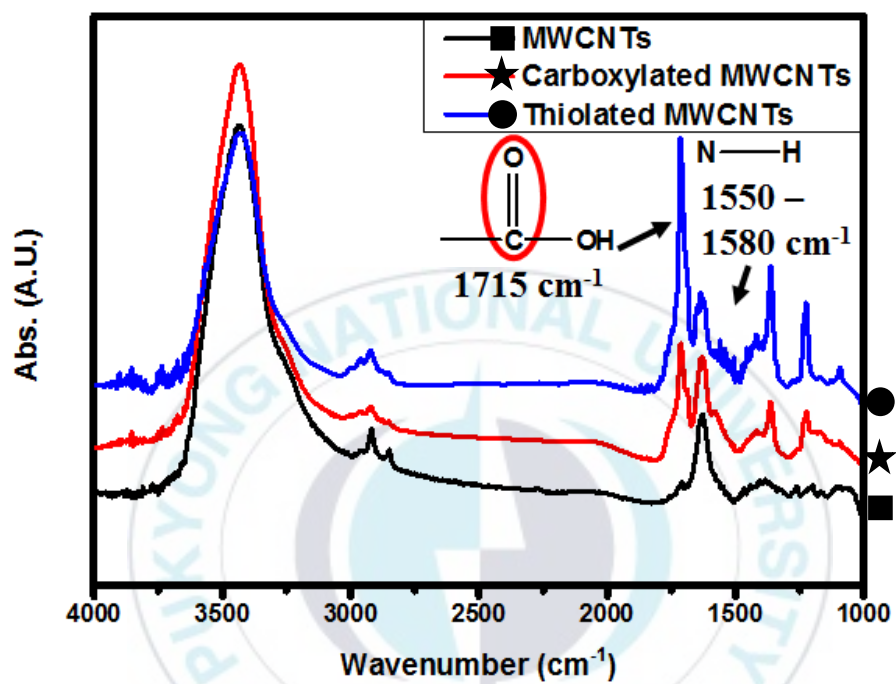


Figure 16. FT-IR spectra of MWCNTs, carboxylated MWCNTs and thiolated MWCNTs.

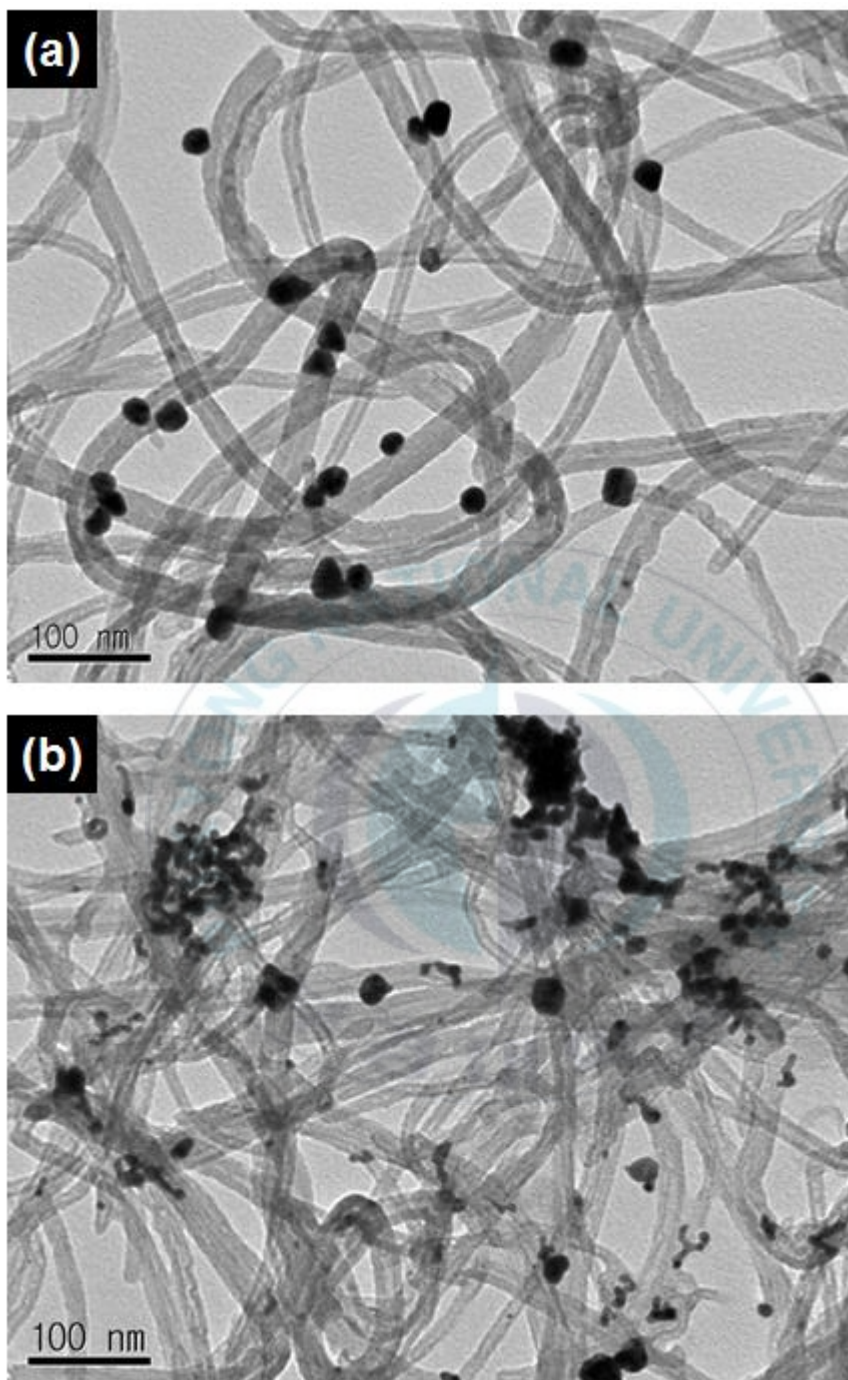


Figure 17. TEM images of the (a) Au NPs attached carboxylated MWCNTs and (b) Au NPs attached thiolated MWCNTs.

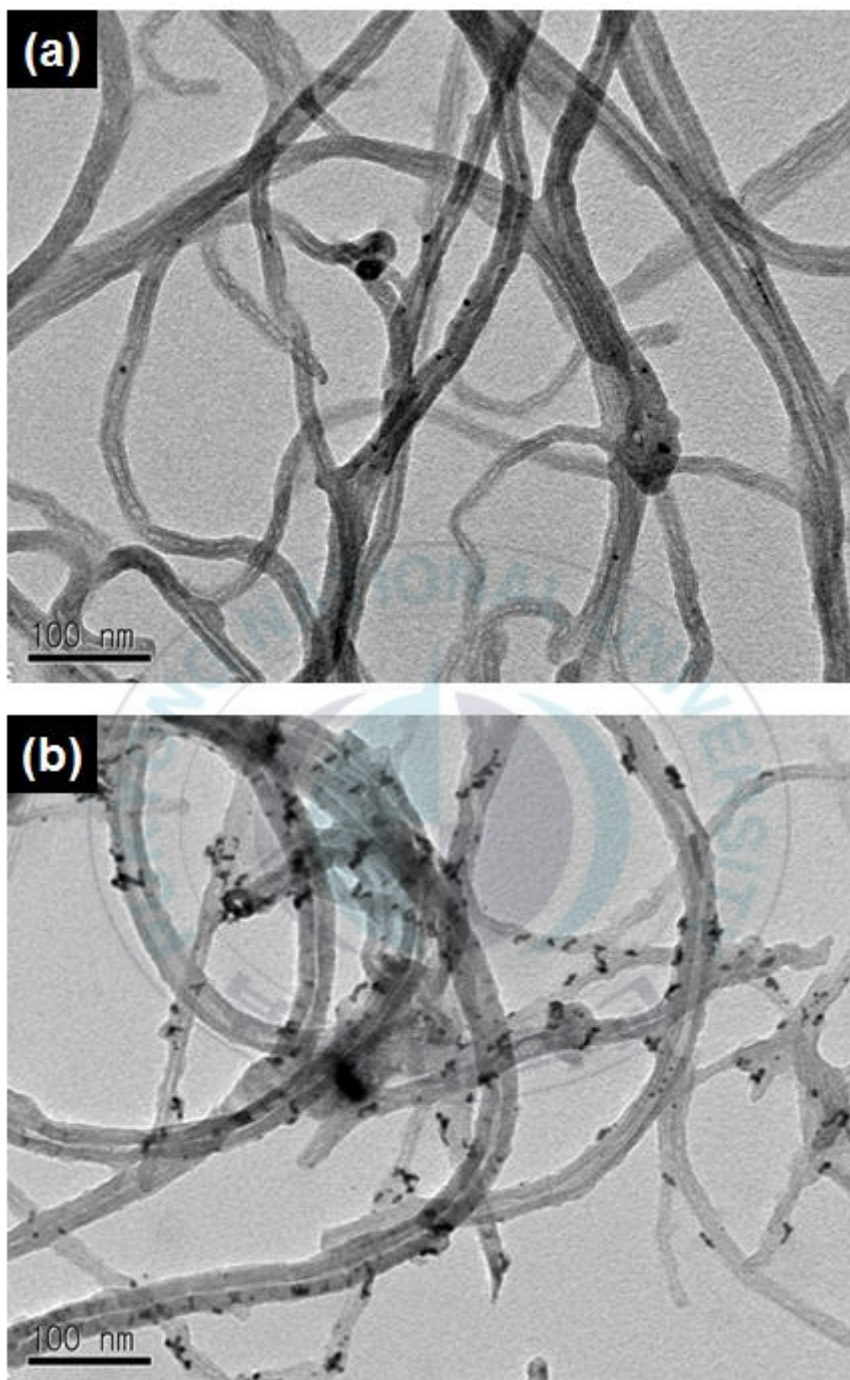


Figure 18. TEM image of the (a) Au NPs attached carboxylated MWCNTs and (b) Au NPs attached thiolated MWCNTs.

In order to improve performance of biosensor, more Au NPs attached MWCNTs was required. Figure 19 is FT-IR spectra of carboxylated MWCNTs with different reflux time. Although reflux time of MWCNTs in 3 M nitric acid was extended, the intensity of absorbance peak corresponding to carboxyl group was not enhanced. Figure 20 shows FT-IR spectra of carboxylated MWCNTs in different concentration of nitric acid. The peak intensity at 1715 cm^{-1} was significantly increased at concentrated nitric acid than 3 M nitric acid.

High concentration of Au NPs solution was required to match with increased thiol group in thiolated MWCNTs and experiments about various parameters such as temperature, amount of gold precursor, capping agent and reducing agent was carried out. Figure 21 is UV-Vis spectra of the prepared Au NPs at $0\text{ }^{\circ}\text{C}$ and room temperature by 4 times more gold precursor and 8 times more capping agent than method introduced in Figure 14(a). The absorbance spectra of prepared Au NPs at $0\text{ }^{\circ}\text{C}$ and room temperature was completely overlapped as shown in Figure 21. In other words, size of Au NPs was independent of reaction temperature. The reaction temperature is factor affecting the reaction rate. However, reduction of HAuCl_4 very quickly proceeds regardless of temperature when using NaBH_4 as reducing agent. Also, the absorbance peak at 533 nm signify very big size of Au NPs. So experiments were conducted as shown in the Table 2, and sample 1, 2 and 3 succeeded in Au NPs synthesis as shown in Figure 22. The others were failed. In case of sample 3, precipitation occurred in process of time. Figure 23(a) is UV-Vis spectra of the measured from the sample 1, 2 and 3. Three absorbance peaks were observed near at 513 nm. Figure 23(b) shows UV-Vis spectrum of sample 2 magnified from Figure 23(a).

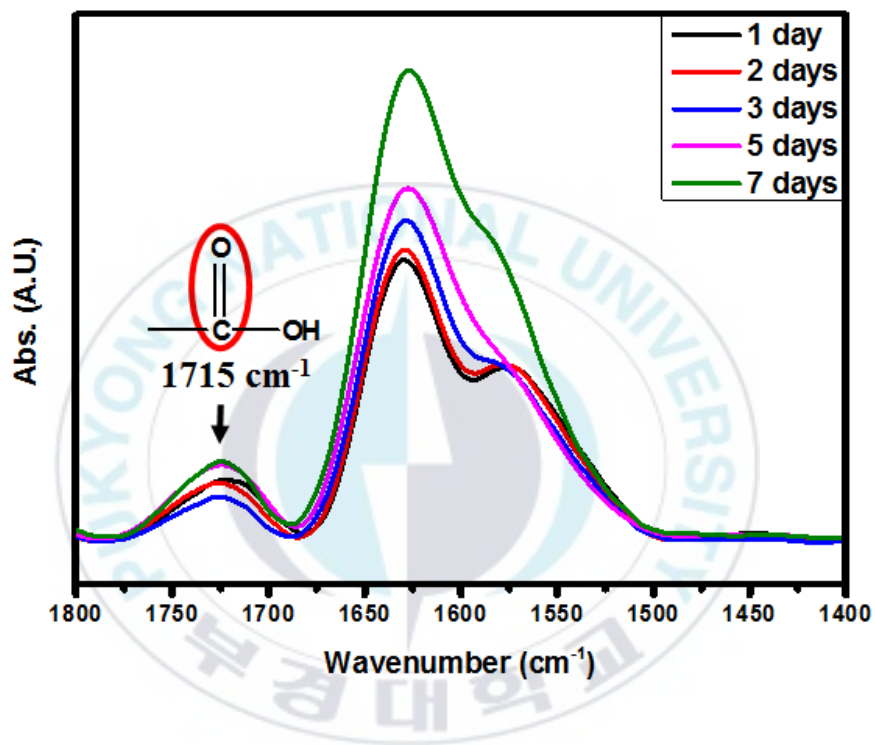


Figure 19. FT-IR spectra of carboxylated MWCNTs with different reflux time.

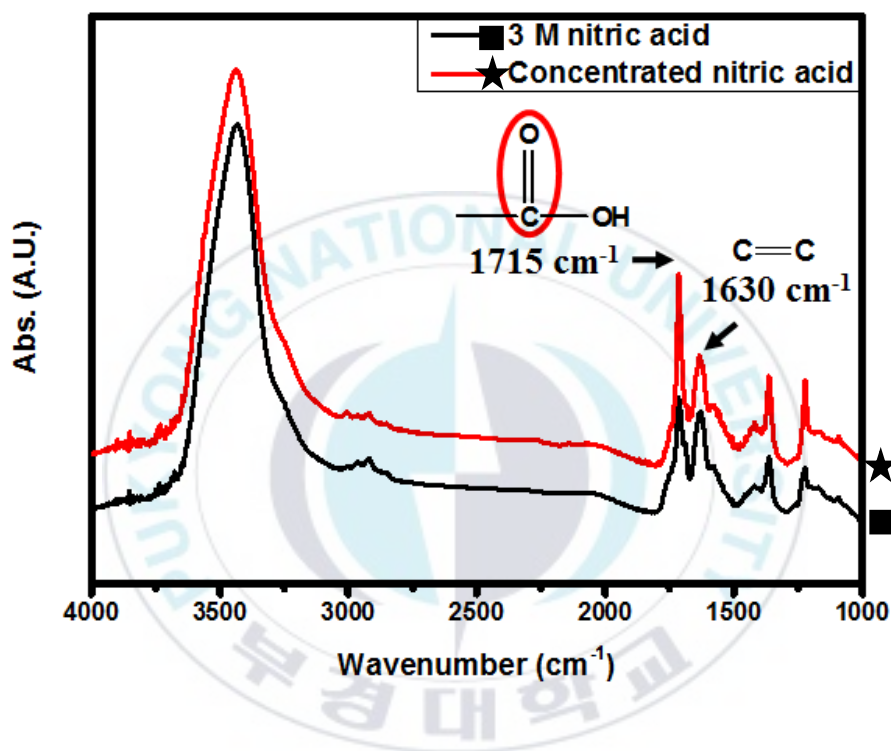


Figure 20. FT-IR spectra of carboxylated MWCNTs according to reflux in different concentration of nitric acid.

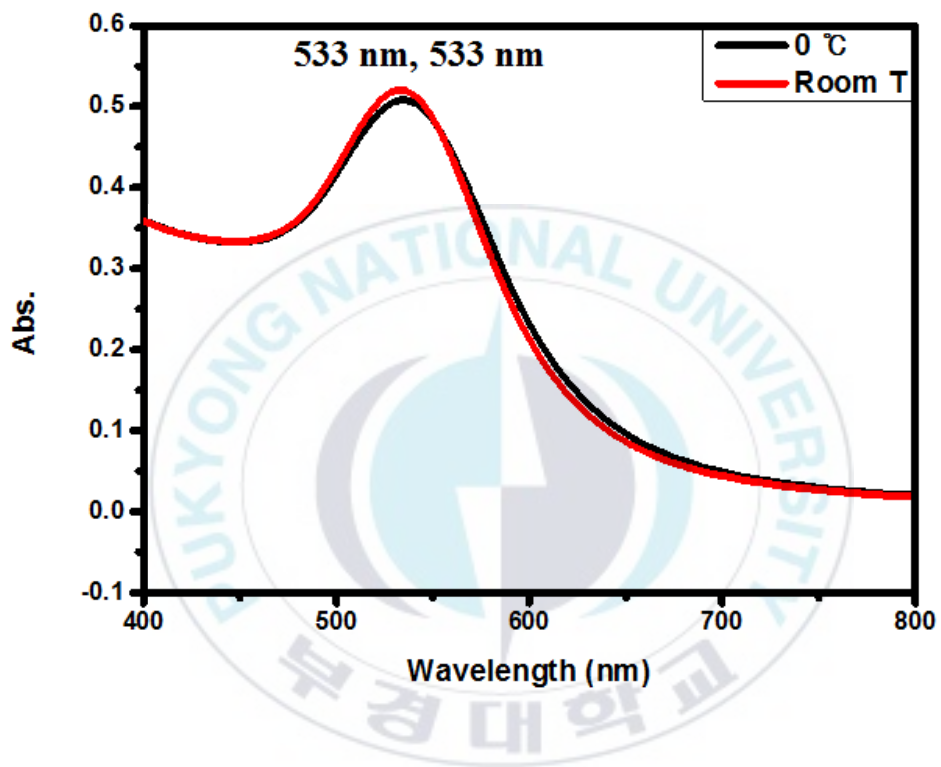


Figure 21. UV-Vis spectra of prepared Au NPs at 0 °C and room temperature.

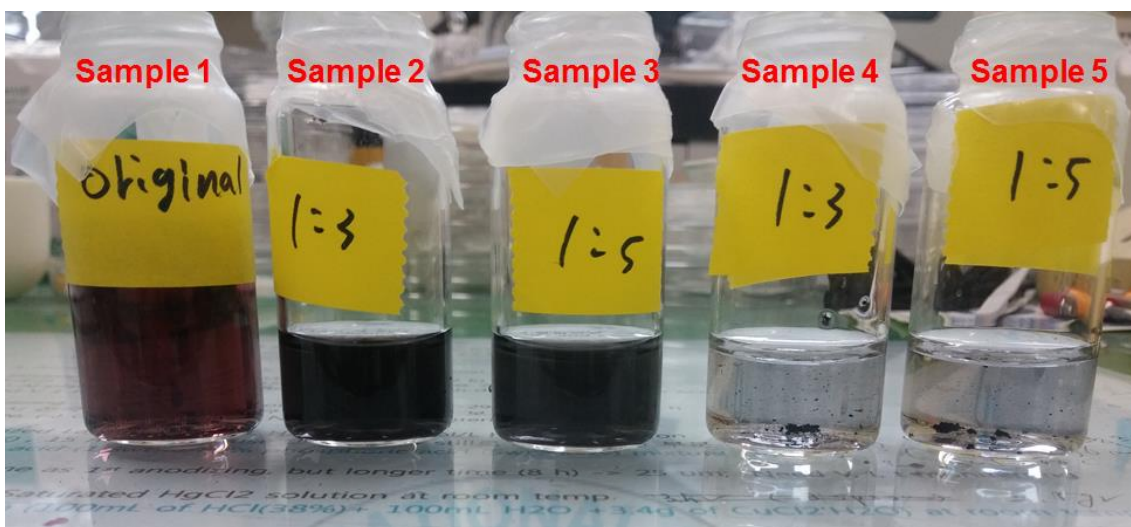


Figure 22. Photograph of the prepared Au NPs solution.

	Sample 1	Sample 2	Sample 3	Sample 4	Sample 5
HAuCl₄	1.25×10^{-6} mol	5×10^{-6} mol	5×10^{-6} mol	5×10^{-6} mol	5×10^{-6} mol
Sodium citrate	1.25×10^{-6} mol	1.5×10^{-5} mol	2.5×10^{-5} mol	1.5×10^{-5} mol	2.5×10^{-5} mol
NaBH₄	1.5×10^{-5} mol	1.5×10^{-5} mol	1.5×10^{-5} mol	6×10^{-5} mol	6×10^{-5} mol
UV-Vis absorbance	513 nm	510 nm	512 nm	×	×

Table 2. The amount of reagents to prepare the Au NPs solution. Total volume of the solution is 5 mL.

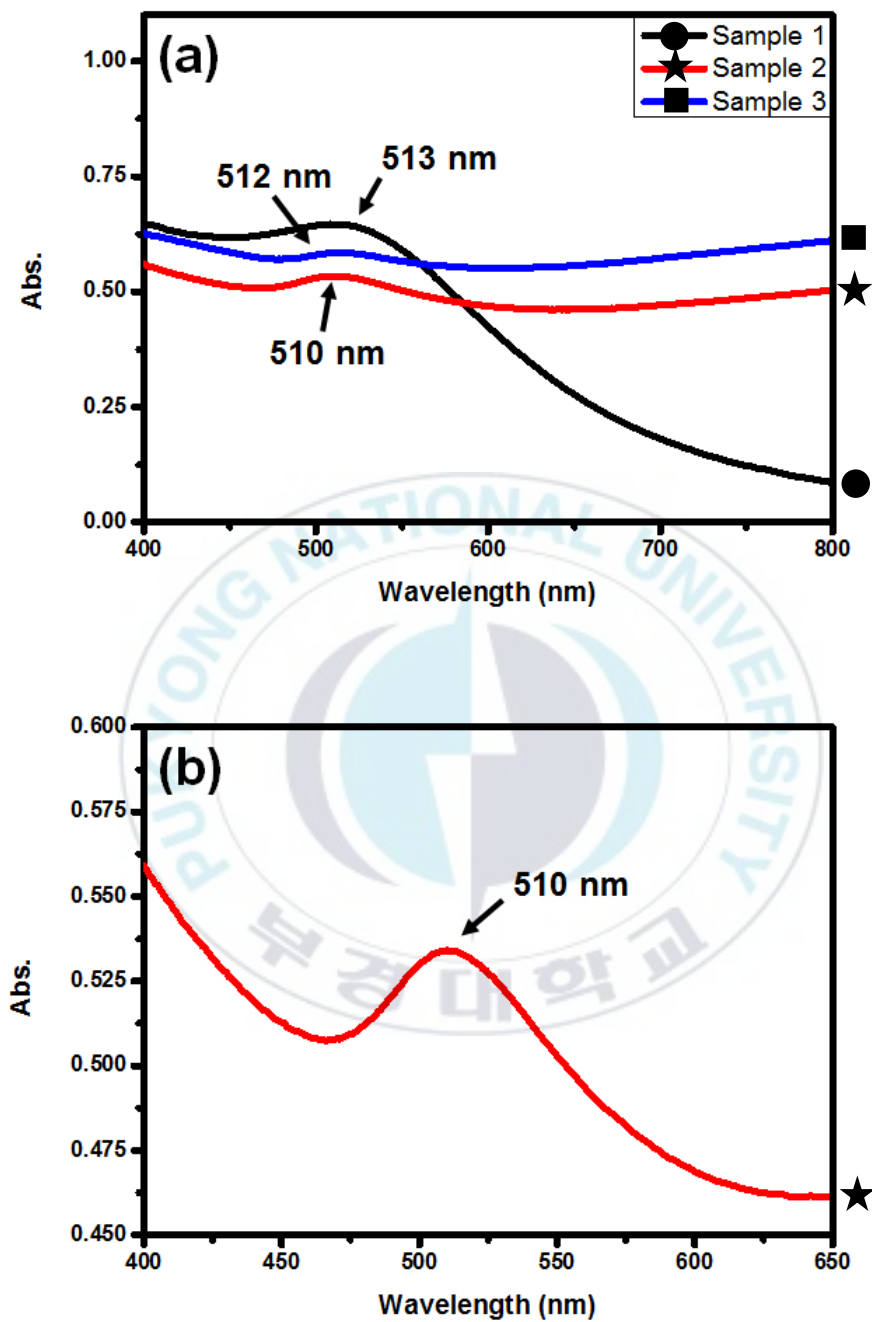


Figure 23. (a) is UV-Vis spectra of sample 1, 2 and 3. (b) is UV-Vis spectrum of sample 2 magnified from Figure 23(a). Total volume of prepared Au NPs solution was 5 mL.

Figure 24 is UV-Vis spectra of prepared Au NPs solution in bulk. The HAuCl₄/sodium citrate/NaBH₄ ratio was 1:3:3 as sample 2 in Table 2 and total volume was 200 mL. Similar to the red line in Figure 15, the absorbance peak was observed at 514 nm. However, in spite of same molar ratio of reagents, it is mismatch with Figure 23(b). Figure 25(a) shows TEM image of prepared Au NPs. The Au NPs had more unequal and bigger size than Au NPs shown in Figure 14(a). The prepared Au NPs had a size distribution as shown in Figure 25(b) and the size of Au NPs was 5.2 nm. Equal maximum stirring speed was applied to the two solution but substantive stirring speed was decreased by increments of solution volume. Figure 26(a), (b) and (c) are TEM image of Au NPs attached MWCNTs. Figure 26(a) shows an overall morphology of Au-MWCNTs and Figure 26(b) shows Au NPs attached to wall of MWCNTs. Crystal lattices from Au NPs and wall of MWCNTs were confirmed in Figure 26(c). The interlayer distance shown in Au NPs was measured to be 0.236 nm, which correspond to (111) lattice plane. Also (002) lattice plane of MWCNT was observed. Figure (d) is SAED (selected area electron diffraction) image of Au NPs. The diffraction rings from inside to outside represent in order MWCNTs (200), Au (111), (200), (220), (311) lattice planes. Au (222) lattice plane was not appeared because of the lack of Au NPs on the surface of MWCNTs.

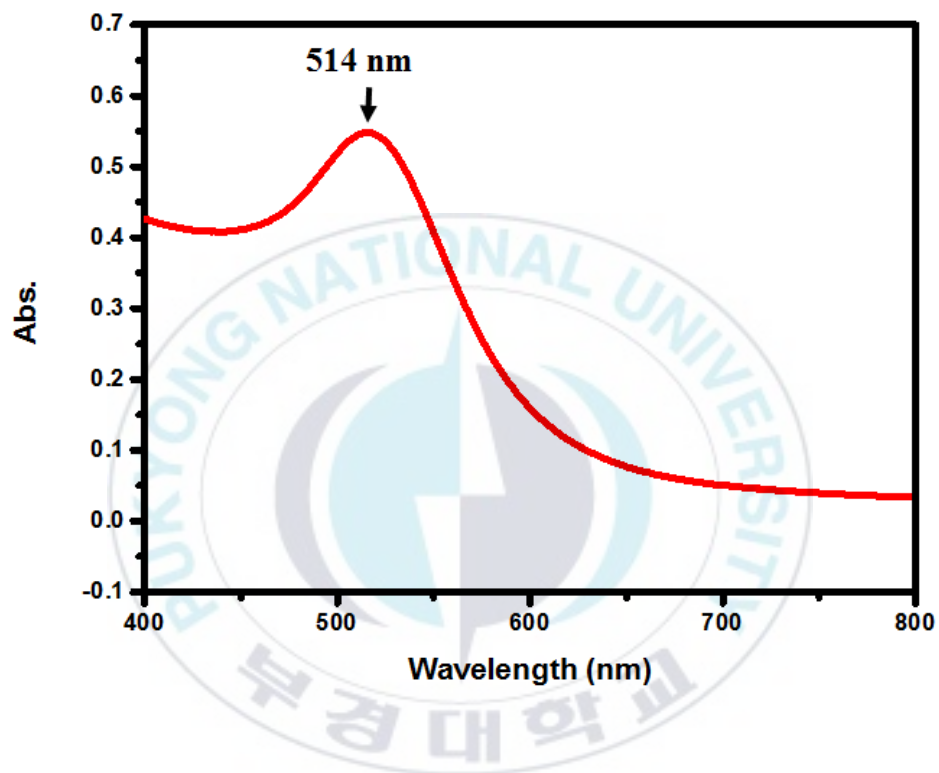


Figure 24. UV-Vis spectra of prepared Au NPs solution in bulk (200 mL).

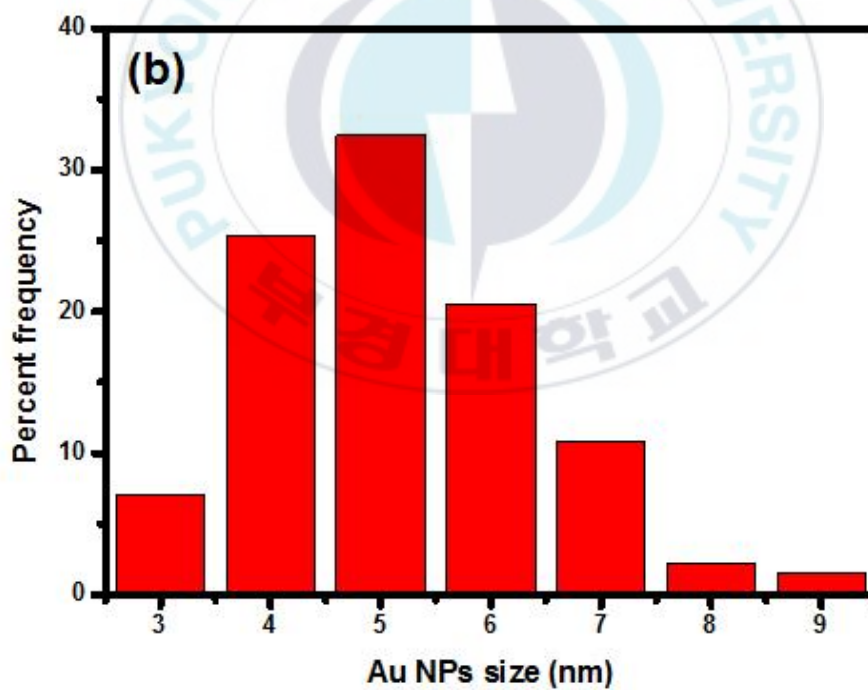
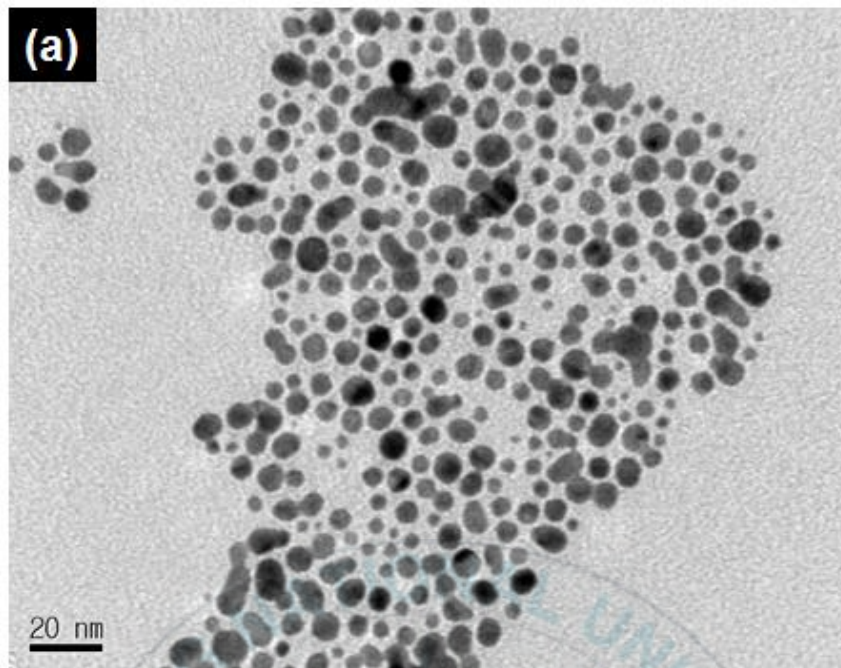


Figure 25. (a) is TEM image obtained from high concentration Au NPs solution in bulk.

(b) is size distribution of Au NPs. (Au NPs size : 5.2 ± 1.2 nm)

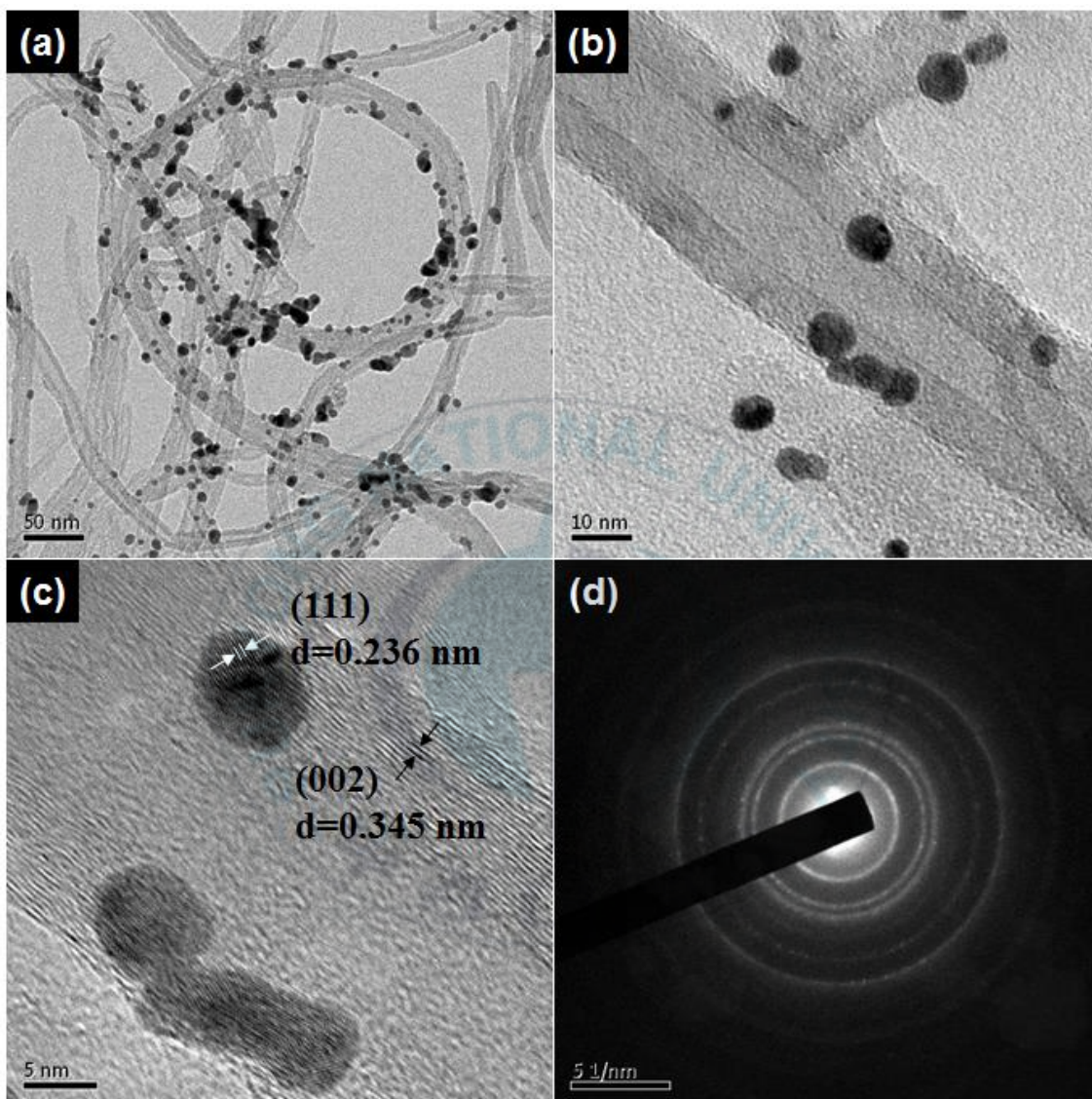


Figure 26. (a) and (b) are TEM images of Au NPs attached MWCNTs. (c) shows crystal lattices of Au NPs and MWCNT wall. (d) is SAED image of Au NPs.

Figure 27 is centrifuging the 1.3 mg of carboxylated MWCNTs and Au-MWCNTs. In spite of same mass, the number of carboxylated MWCNTs and Au-MWCNTs was different because of weight of Au NPs. As discussed above 1.3 mg of carboxylated MWCNTs is optimum amount to obtain uniform Ab-MWCNTs deposited sensing paper. However, 1.4 mg was optimum amount for Au-MWCNTs based sensing paper. Thickness of Ab-Au-MWCNTs layer in sensing paper without filter paper was confirmed to be about 2 μm by alpha-step as shown in Figure 28. Ab-Au-MWCNTs layer loaded on the filter paper was thinner, more compact and uniform than Ab-MWCNTs layer. It is because dispersion power in water is enhanced by attaching the Au NPs to MWCNTs. As previously mentioned, uniformity of functionalized MWCNTs deposited on filter paper is proportional to dispersion power in water. Figure 29 is the electrical signals of biosensor for blank samples. The standard deviation estimated from Figure 29 was 2×10^{-3} . This value is 1.5 times less than Ab-MWCNTs based sensing paper (standard deviation: 3×10^{-3}). Figure 30 shows resistance variation according to PSA concentration. Actually, the performance of biosensor based on Au-MWCNTs was disappointing. Success rate of PSA detection was low and the data shown in Figure 30 was obtained with difficulty. Also, when comparing Figure 12(a) and Figure 30, expecting improved sensitivity is difficult. Despite superior uniformity of sensing materials deposited on the filter paper and increase of reaction site with PSA, the performance of biosensor deteriorated. As discussed above, increase of electrical resistance according to increased PSA concentration is due to the increments of distance between functionalized MWCNTs by combination of PSA and functionalized MWCNTs. In case of Au-MWCNTs based biosensor, sensing materials layer consist of high-density Ab-Au-MWCNTs. The high compactness disrupt permeation of PSA between Ab-Au-MWCNTs.

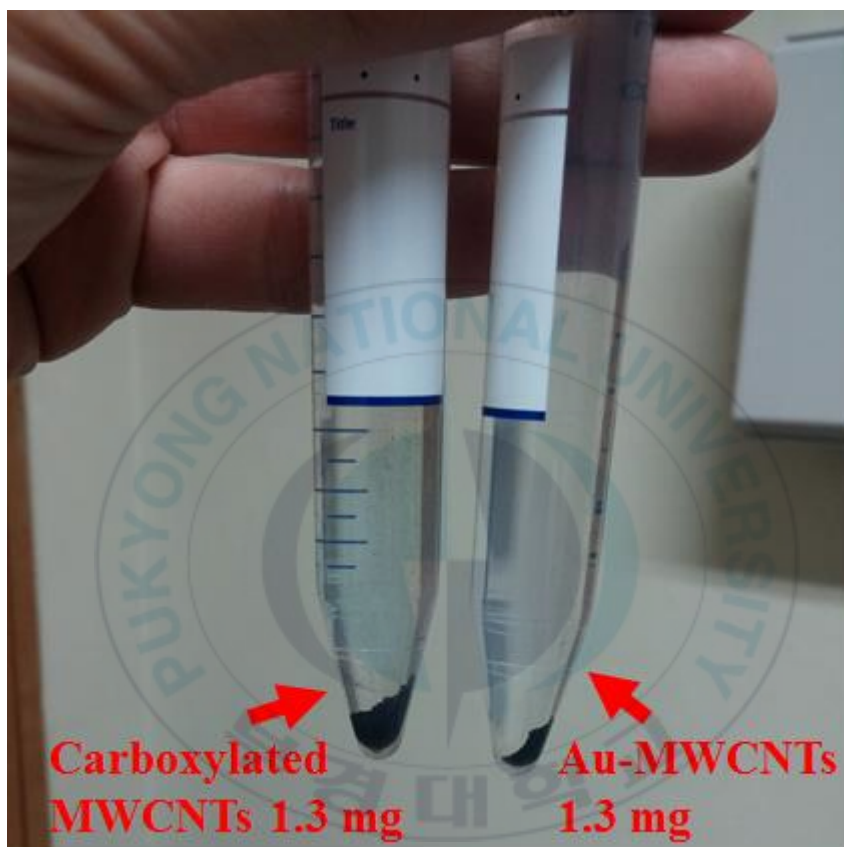


Figure 27. Compared specific gravity between carboxylated MWCNTs and Au-MWCNTs.

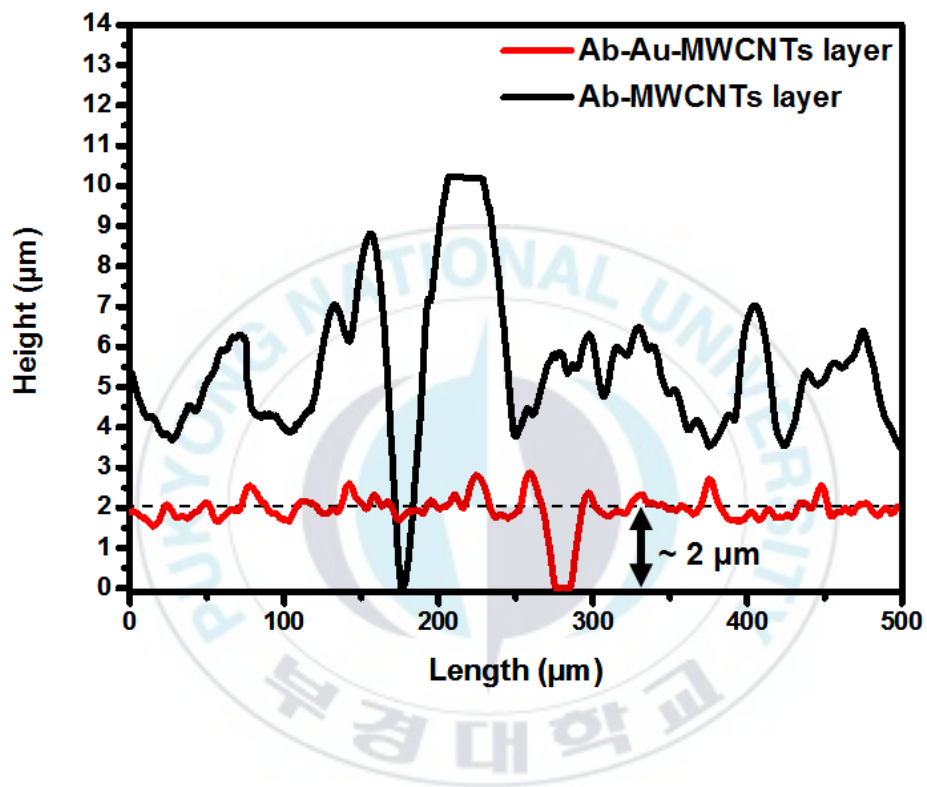


Figure 28. Height profile measured by alpha-step. Thickness of Ab-Au-MWCNTs layer measured after removing the filter paper.

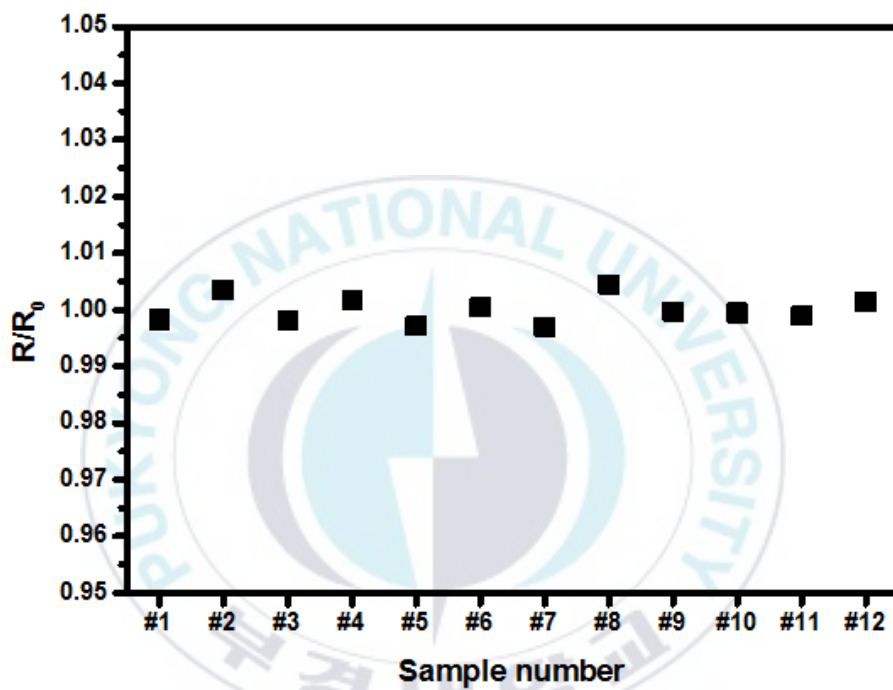


Figure 29. Electrical signal of background to determine the detection limit.

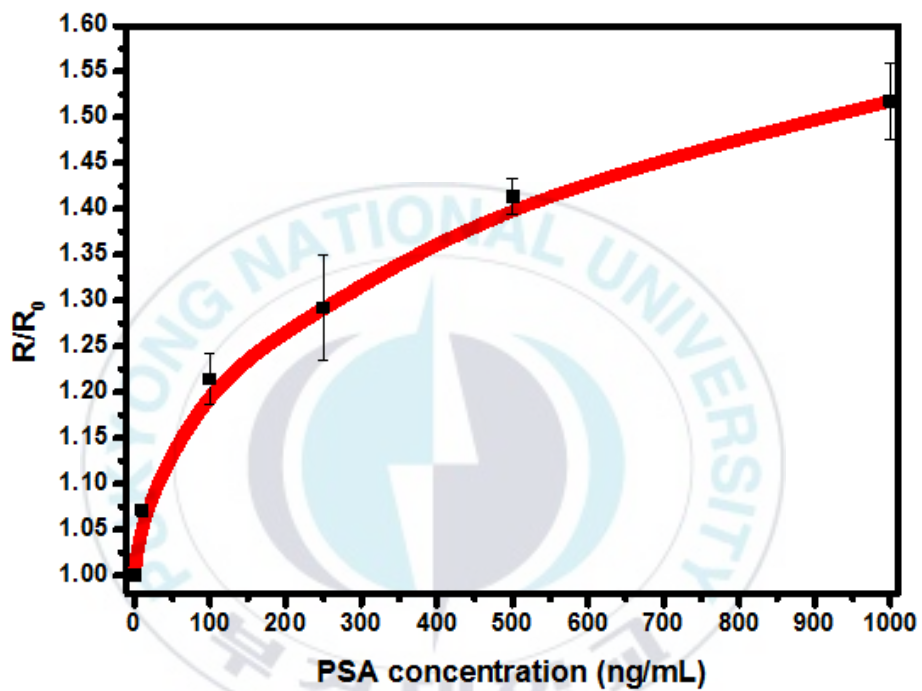
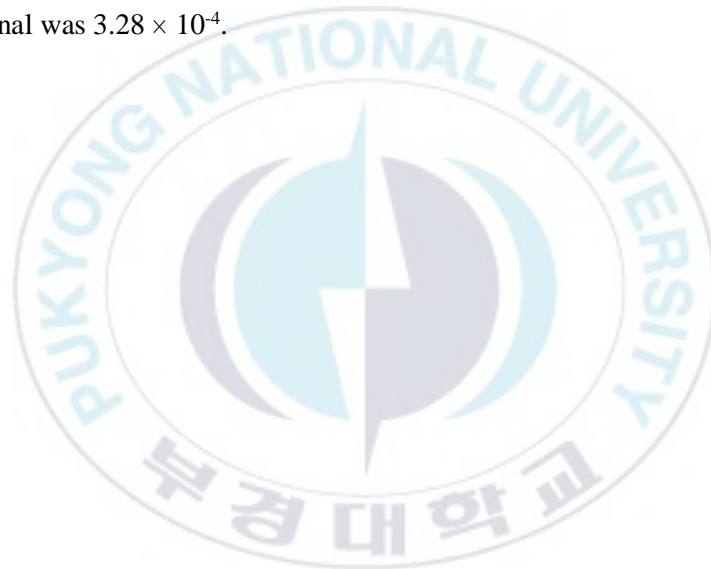


Figure 30. The plot of relative resistance vs. PSA concentration. PSA concentration is 0, 10, 100, 250, 500 and 1000 ng/mL.

3.3 Commercial ELISA kit performance test

Figure 31 (a) shows optical density according to PSA concentration. The optical density was increased nearly linearly along with the increased concentration of PSA from 0 ng/mL to 5 ng/mL as shown in Figure 31(b). When the concentration of the PSA is more than 5 ng/mL, signal vs. PSA concentration lost linearity. The detection limit estimated, which was measured by $2 \times$ standard deviation of mean value of signals estimated from three control well (without PSA), was 51 pg/mL. The standard deviation of blank signal was 3.28×10^{-4} .



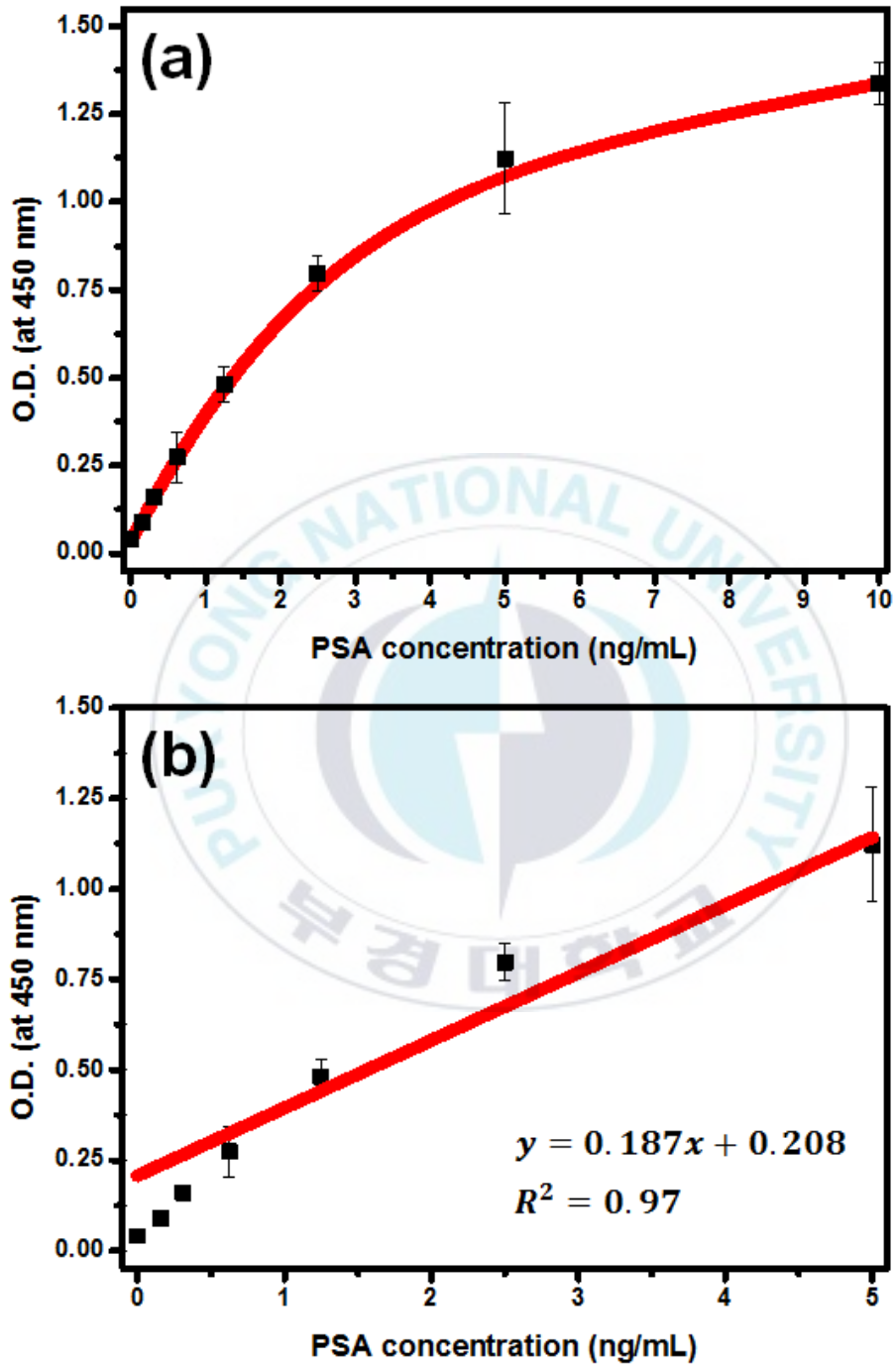


Figure 31. (a) Optical density of ELISA method at 450 nm vs. PSA concentration. (b) Linear range of signal along with PSA concentration at ELISA method.

4. Conclusion

We have successfully demonstrated fabrication of pragmatic sheet-type biosensor based on carboxylated MWCNTs and micro-pore filter paper for early detection of prostate cancer. According to increase of PSA concentration from 0 ng/mL to 500 ng/mL, electrical resistance was increased up to 150% nearly linearly. Maximum detection range of the biosensor was 500 ng/mL and detection limit was 1.18 ng/mL. The sheet-type biosensor based on carboxylated MWCNTs is 23 times cheaper (fabricated biosensor price: 2.4 \$) and 12 times faster than ELISA based method used in hospital, which is general method for the detection of a specific protein. Furthermore, the maximum detection level is about 100 times higher than ELISA. Detection limit and sensitivity of the prepared biosensor are sufficient to diagnose the early stage of prostate cancer (>4 ng/mL of PSA). The sensor can detect various biomolecules as well as PSA by using bio-specific materials combined CNTs, those react only with target biomolecules. We believe this handy bio-sensing procedure could be a very useful diagnosis tool for various fatal diseases in underdevelopment countries or hinterland, where medical system is poorly equipped, not far future.

The biosensor based on Au-MWCNTs was predicted to remarkable progress because of superior uniformity of sensor element deposited on the filter paper by increased reaction site and excellent dispersion power of Au-MWCNTs in water. However, excessive uniformity of sensor element was more of a hindrance than a help to improve the sensitivity of biosensor. PSA did not enter between the Ab-Au-MWCNTs because of compact sensor element. As a result, Au-MWCNTs based biosensor did not function as biological sensing system. In order to overcome the

problem, more research and development is required.



5. References

1. Rebecca, S.; Jiemin, M.; Zhaohui, Z.; Ahmedin J. Cancer Statistics, 2014. CA. CANCER J CLIN. **2014**, 64, 9-29.
2. Kyu-Won, J.; Young-Joo, W.; Hyun-Joo, K.; Chang-Mo, O.; Duk Hyung, L.; Jin Soo, L. Cancer Statistics in Korea: Incidence, Mortality, Survival, and Prevalence in 2011. Cancer Res Treat. **2014**, 46(2), 109-123.
3. Ian, M.T.; Donna, P.A. Prostate-specific antigen in the early detection of prostate cancer. CMAJ. **2007**, 176(13), 1853-1858.
4. Stacey, F.; Ann, G.S. Cancer Prevention & Early Detection Facts & Figures 2015-2016. American Cancer Society. **2015**.
5. Kyle, S.; Jorge, A.; Tavel, M.D. What are Biomarkers?. **2010**, 5(6), 463-466.
6. Anant, N.B.; Rohit, M.; Abdullah, F.; Amit, V.; Dwarakanath, B.S. Cancer biomarkers-Current perspectives. INDIAN J MED RES. **2010**, 132, 129-149.
7. Hara, M.; Inorre, T.; Fukuyama, T. Some physicochemical characteristics of gamma-seminoprotein, an antigenic component specific for human seminal plasma. Jpn J Legal Med. 1971, 25, 322-324.
8. Lawrence, D.P.; Ming, C.W.; Luis, A.V. A Prostate Antigen in Sera of Prostatic Cancer Patients. CANCER RESEARCH. 1980, 40, 2428-2432.
9. Ian, M.T.; Donna, K.P., Phyllis, J.G.; Catherine, M.T.; Scott, L.; Howard, L.P.; Lori, M.M.; Leslie, G.F.; Scott, M.L.; David, C.; John, J.C.; Charles, A.C. Prevalence of Prostate Cancer among Men with a Prostate-Specific Antigen Level ≤ 4.0 ng per Milliliter. N Engl J Med. **2004**, 350, 2239-2246.

10. Dianna, E.V.O. Enzyme-linked immunosorbent assay (ELISA) Quantitative assay of immunoglobulin G. *Immunochemistry*. **1971**, 8, 871-874.
11. Leena, I.S.; Lionel, E.S.; Keith, H. AN ENZYME-LINKED IMMUNOSORBENT ASSAY (ELISA) FOR PROSTATE-SPECIFIC ANTIGEN. Elsevier. **1991**, 50, 125-138.
12. Gabriela, G.G.; Jose, L.H. Sandwich-type ELISA impedimetric immunosensor for early detection of prostate-specific antigen (PSA) in human serum. *Procedia chemistry*. **2014**, 12, 47-54.
13. Tsu-Lan, W.; Yu-Chen, S.; Pi-Yueh, C.; Kuo-Chien, T.; Chien-Feng, S.; James T, W. Establishment of ELISA on 384-Well Microplate for AFP, CEA, CA 19-9, CA 15-3, CA 125, and PSA-ACT: Higher Sensitivity and Lower Reagent Cost. *Journal of Clinical Laboratory Analysis*. **2003**, 17, 241-246.
14. Napat, T.; Papot, J.; Haibin, S.; Joanne, I.Y.; Roderic, B. Microfluidic chip-based nanoelectrode array as miniaturized biochemical sensing platform for prostate-specific antigen detection. *Biosensors and Bioelectronics*. **2011**, 26, 2927-2933.
15. Ludan, W.; Meng, L.; Meng, Z.; Mei, Y.; Shenguang, G.; Jinghua, Y. Ultrasensitive electrochemiluminescence immunosensor for tumor marker detection based on nanoporous silver@carbon dots as labels. *Sensors and Actuators B*. **2013**, 186, 761-767.
16. Shun, M.; Ganhua, L.; Kehan, Y.; Junhong, C. Specific biosensing using carbon nanotubes functionalized with gold nanoparticle-antibody conjugates. *Carbon*. **2010**, 48, 479-486.

17. Desiree, S.G.; Robert J.L.; Hye-Young, P.; Jeremy, D.; Marc D.P. Femtomolar Detection of Prostate-Specific Antigen: An Immunoassay Based on Surface-Enhanced Raman Scattering and Immunogold Labels. *Anal. Chem.* **2003**, *75*, 5936-5943.
18. Hee-Jo, L.; Jung-Hyun, L.; Hui-sung, M.; Ik-Soon, J.; Jong-Soon, C.; Jong-Gwan, Y.; Hyo-II, J. A planar split-ring resonator-based microwave biosensor for label-free detection of biomolecules. *Sensors and Actuators B.* **2012**, *169*, 26-31.
19. Sumio, I.; Toshinari, I. Single-shell carbon nanotubes of 1-nm diameter. *Nature.* **1993**, *363*, 603-605.
20. Ray, H.B.; Anva, A.Z.; Walt, A.de H.; Carbon Nanotubes—the Route Toward Applications. *Science.* **2002**, *297*, 787-792.
21. Ali, E.; Hadis, D.; Hamzeh, K.; Mohammad, K.; Nosratollah, Z.; Abolfazl, A.; Mozghan, A.; Younes, H.; Sang Woo, J. Carbon nanotubes: properties, synthesis purification, and medical applications. *Nanoscale Research Letters.* **2014**, *9*, 393-405.
22. Sumio, I. Helical microtubules of graphitic carbon. *Nature.* **1991**, *354*, 56-58.
23. Michael, F.L.D.V.; Sameh H.T.; Ray, H.B.; John, H. Carbon Nanotubes: Present and Future Commercial Applications. *Science.* **2013**, *339*, 535-539.
24. Rodney, S.R.; Dong, Q.; Wing Kam, L. Mechanical properties of carbon nanotubes: theoretical predictions and experimental measurements. *C. R. Physique.* **2003**, *4*, 993-1008.
25. Hongjie, D. Carbon Nanotubes: Synthesis, Intergration, and Properties. *Acc. Chem. Res.* **2002**, *35*, 1035-1044.

26. Xi-Liang, L.; Jing-Juan, X.; Jin-Li, W.; Hong-Yuan, C. Electrochemically deposited nanocomposite of chitosan and carbon nanotubes for biosensor application. *Chem. Commun.* **2005**, 2169-2171.
27. Wenrong, Y.; Kyle, R.R.; Simon, P.R.; Pall, T.; J, J.G.; Filip, B. Carbon Nanomaterials in Biosensors: Should You Use Nanotubes or Graphene?. *Angew. Chem. Int. Ed.* **2010**, 49, 2114-2138.
28. Celine I.L., J.; Teresa A.P., R.S.; Armando C., D. Advances in point-of-care technologies with biosensors based on carbon nanotubes. *Trends in Analytical Chemistry.* **2013**, 45, 24-36.
29. Abdollah, S.; Begard, K.; Farden, F.; Rahman, H. Highly sensitive immunosensing of prostate-specific antigen based on ionic liquid-carbon nanotubes modified electrode: Application as cancer biomarker for prostate biopsies. *Biosensors and Bioelectronics.* **2013**, 42, 439-446.
30. Fang, L.; Wenping, D.; Yan, Z.; Shenguang, G.; Jinghua, Y.; Xianrang, S. Application of ZnO quantum dots dotted carbon nanotube for sensitive electrochemiluminescence immunoassay based on simply electrochemical reduced Pt/Au alloy and a disposable device. *Analytica Chimica Acta.* **2014**, 818, 46-53.
31. Jun, P.K.; Byung, Y.L.; Joohyung, L.; Seunghun, H.; Sang, J.S. Enhancement of sensitivity and specificity by surface modification of carbon nanotubes in diagnosis of prostate cancer based on carbon nanotube field effect transistors. *Biosensors and Bioelectronics.* **2009**, 24, 3372-3378.
32. Shah, M.Z.H. The teenage scientist revolutionizing cancer detection. *Bangladesh Med J.* **2013**, 42(2), 71.

33. Elad, S.; Jingli, Z.; Kevin, H.; Seth M., S.; Ira, P.; Masanori, O.; Jochen, G.; B. Michael, G.; Thomas, R.; Raffit, H. Serum mesothelin and megakaryocyte potentiating factor in pancreatic and biliary cancers. *Clin Chem Lab Med.* **2011**, 50(4), 721-725.
34. [Http://en.wikipedia.org/wiki/Jack_Andraka](http://en.wikipedia.org/wiki/Jack_Andraka)
35. Tao, J. The electric field screening and crossing point shift effects in coated carbon nanotubes. *Appl. Phys. A.* **2014**, 116, 629-633.
36. Xin, Y.; Bernard, M.; Vyomesh, P.; Gary, J.; Ashwin, B.; Joseph D., G.; Sang N., K.; John, G.; J. Silvio, G.; Fotios, P.; James F., R. Carbon Nanotube Amplification Strategies for Highly Sensitive Immunodetection of Cancer Biomarkers. *J. AM. CHEM. SOC.* **2006**, 128, 11199-11205.
37. YeoHeung, Y.; Adam, B.; William R., H.; H. Brian, H.; Vesselin N., S.; Zhongyun, D.; Sarah, P.; Michael, B.; Abdul, J.; Yi, T.; Danny K.Y., W.; Amit, B.; Mark J., S. A nanotube array immunosensor for direct electrochemical detection of antigen-antibody binding. *Sensors and Actuators B.* **2007**, 123, 177-182.
38. Maelle, P.; Anthony, T.; Arben, M. Cancer detection using nanoparticle-based sensors. *Chem. Soc. Rev.* **2012**, 41, 2606-2622.
39. Daxiang, C.; Bifeng, P.; Hong, Z.; Feng, G.; Rina, W.; Jingping, W.; Rong, H.; Toru, A. Self-Assembly of Quantum Dots and Carbon Nanotubes for Ultrasensitive DNA and Antigen Detection. *Anal. Chem.* **2008**, 80, 7996-8001.
40. Gary C., J.; Xin, Y.; Joseph D., G.; Bernard, M.; Ashwin, B.; Sang N., K.; Fotios, P.; James F., R. Characterization of Multienzyme-Antibody-Carbon Nanotube Bioconjugates for Immunosensors. *J Nanosci Nanotechnol.* **2009**, 9(1), 249-255.

41. Jae, H.J.; Doo, S.C.; Fei, L.; Kang Bum, L.; Tae, S.S. A Graphene Oxide Based Immuno-biosensor for Pathogen Detection. *Angew. Chem. Int. Ed.* **2010**, *49*, 5708-5711.
42. Juan, T.; Dianping, T.; Biling, S.; Jianxin, H.; Bin, Q.; Guonan, C. Enzyme-free electrochemical immunoassay with catalytic reduction of p-nitrophenol and recycling of p-aminophenol using gold nanoparticles-coated carbon nanotubes as nanocatalysts. *Biosensors and Bioelectronics.* **2011**, *26*, 3219-3226.
43. Vigneshwaran, M.; Bhaskara V., C.; Vyomesh, P.; J. Silvio, G.; James F., R. Ultrasensitive Immunosensor for Cancer Biomarker Proteins Using Gold Nanoparticle Film Electrodes and Multienzyme-Particle Amplification. *ACS NANO.* **2009**, *3*, 585-594.
44. James F., R.; Gregory, S.; Fotios, P. Designing nanomaterial-enhanced electrochemical immunosensors for cancer biomarker proteins. *Bioelectrochemistry.* **2009**, *76*, 189-194.
45. Shi-fang, R.; Yin-long, G. Oxidized carbon nanotubes as matrix for matrix-assisted laser desorption/ionization time-of-flight mass spectrometric analysis of biomolecules. *Rapid Commun. Mass Spectrom.* **2005**, *19*, 255-260.
46. Huan, N.; Ruo, Y.; Yaqin, C.; Li, M.; Yali, Y.; Yaling, C.; Ying, Z. Highly enhanced electrochemiluminescence based on synergetic catalysis effect of enzyme and Pd nanoparticles for ultrasensitive immunoassay. *Chem. Commun.* **2011**, *47*, 8397-8399.

47. Bei, L.; Lingsong, L.; Erhui, H.; Shuting, J.; Guoming, X. Detection of the human prostate-specific antigen using an aptasensor with gold nanoparticles encapsulated by graphitized mesoporous carbon. *Microchim Acta*. **2012**, 178, 163-170.
48. Nitin, C.; Mainak, M.; Bruce J., H. Bifunctional Carbon Nanotubes by Sidewall Protection. *Adv. Funct. Mater.* **2005**, 15, 858-864.
49. Colin, D.B.; E. Barry, T.; Yu-Tai, T.; Joseph, E.; George M., W.; Ralph G., N. Formation of Monolayer Films by the Spontaneous Assembly of Organic Thiols from Solution onto Gold. *J. Am. Chem. Soc.* **1989**, 111, 321-335.
50. Ami, E.; Kuiyang, J.; Doug, D.; Rodney, A.; Linda S., S. Surface Modification of Multiwalled Carbon Nanotubes: Toward the Tailoring of the Interface in Polymer Composites. *Chem. Mater.* **2003**, 15, 3198-3201.
51. Ansoon, K.; Chil, S.A.; Han, Y.Y.; Jong-Heon, Y.; In-Bok, B.; Chang-Guen, A.; Chan, W.P.; Myung, S.J. Ultrasensitive, label-free, and real-time immunodetection using silicon field-effect transistors. *Appl. Phys. Lett.* **2007**, 91, 103901-103903.
52. Nikhil R., J.; Latha, G.; Catherine J., M. Wet Chemical Synthesis of High Aspect Ratio Cylindrical Gold Nanorods. *J. Phys. Chem. B.* **2001**, 105, 4065-4067.
53. Mohamed, A.K.A.; Mohsen, M.M.; Magdy, M.G. Physical Properties of Different Gold Nanoparticles: Ultraviolet-Visible and Fluorescence Measurements. *J Nanomed Nanotechol.* **2012**, 3.

감사의 글

지난 2년간 바이오센서 개발에 대해 연구한 결과를 바탕으로 이 학위 논문이 나왔습니다. 한 분야에 대해 연구하고 실험하여 만족스러운 결과를 얻는데 2년이라는 시간은 너무 짧았습니다. 미흡하지만 이만큼의 성과를 낸 것은 항상 도움을 주신 화학과와 여러 교수님들과 선배님, 후배, 동기가 있었기에 가능했습니다.

먼저 부족한 저의 지도교수님이 되어주시고 2년 동안 저를 이끌어주신 김돈 교수님께 감사드립니다. 항상 어려운 길을 권하고, 스스로 생각하고, 해결하기를 원하시는 교수님께 원망스럽고, 불만스러운 감정이 많았던 것 같습니다. 지치고 힘들어 포기하고 싶었습니다. 하지만 교수님께서 끝까지 저를 기다려주셨고, 만족스럽지 못한 결과에서 가능성을 언급하시며 격려해 주셨습니다. 교수님께서 연구에 대한 지식 이외에도 스스로 생각하고, 판단하여 문제를 해결해 나가고, 불가능과 부정적인 결과로부터 가능성을 찾는 연습을 시켜 제가 졸업한 후 삶을 살아가면서 수많은 역경과 고난에 부딪혔을 때 스스로 극복해 나가는 힘을 길러주고자 하신 것임을 지금에서야 깨달았습니다. 이러한 교수님의 가르침 덕분에 항상 부정적인 시선으로만 세상을 바라보던 제가 조금이나마 긍정적이고 능동적인 사람이 될 수 있었습니다. 또한 부족한 제 논문을 심사해 주시고 따뜻한 격려와 충고를 아끼지 않으신 장병용 교수님과 곽민석 교수님께 감사드립니다.

그리고 끊임없이 저의 문제점과 나아갈 방향에 대해 말씀해주신 이명순 박사님께 감사드립니다. 박사님의 풍부한 경험과 체계적이고 논리적인 판단에서 많은 것을 배울 수 있었습니다. 항상 저에게 궁금하지 않니? 재미있지 않니? 라는 질문을 던져주시며 실험에 대한 호기심과 애정이 있어야 한다고 말씀하셨습니다. 제가 어렸을 때 꿈꿔왔던 과학자의 모습이 지금의 이명순 박사님과 같았습니다. 그래서 겉으로 표현은 하지 않았지만 항상 존경하였습니다. 2년 동안 정말 감사했습니다.

석사 생활을 하며 스스로의 한계를 느끼고, 몸도 마음도 힘들고 지쳐 자존감이 바닥을 드러내고, 모든 것을 내려놓고 포기하고 싶을 때 다시한 번 일어 설 수 있게 해준 전다솜에게 감사하는 마음을 전하고 싶습니다.

끝으로 생화학에 대한 지식이 전혀 없는 저에게 실험적으로 많은 도움을 준 장인승, 정승현, 항상 긍정적인 말로 힘을 준 정은강, 박희선, 그 밖에 많은 대학원생들, 2년 동안 한결같이 저를 믿고 응원해준 가족에게 감사의 말씀전해 올립니다. 감사합니다.

